

On Shear Stress Distributions for Flow
in Smooth or Partially Rough Annuli

B. Kjellström and S. Hedberg



AKTIEBOLAGET ATOMENERGI

STOCKHOLM, SWEDEN 1966

ERRATUM

to report AE-243

On shear stress distributions for flow in smooth or partially
rough annuli

B Kjellström and S Hedberg
(Published 1966)

Page 10: Eq:s (I-28), (I-29) and (I-30).

The denominator should read

$$2\pi r^2$$

ON SHEAR STRESS DISTRIBUTIONS FOR FLOW IN SMOOTH
OR PARTIALLY ROUGH ANNULI

B Kjellström and S Hedberg

SUMMARY

It is commonly assumed that for turbulent flow in annuli the radii of zero shear and maximum velocity are coincident. By inspection of the differential equations for such flow and by an integral analysis it is shown that this is not necessarily true.

To check whether important differences could occur, experiments were made in which velocity and shear stress distributions were measured in one smooth and two partially rough annuli. The results show no difference in the radii for the smooth annulus, but for the partially rough annuli there was a small but significant difference. This difference explains the breakdown of Hall's transformation theory reported by other investigators.

The error introduced by use of Hall's theory is however small, of the order of 10 % or less.

Printed and distributed in August, 1966

LIST OF CONTENTS

	<u>Page</u>
Part I Theoretical considerations	
1. Introduction	3
2. Basic equations	4
2.1 General equations	4
2.2 Transformation to cylindrical coordinates	5
2.3 Application to steady flow in annuli with constant cross-section area	6
3. Calculation of the radius of zero shear	7
4. Integral analysis of the conditions at the radius of maximum velocity	9
5. Conclusions from the theoretical considerations	11
6. Nomenclature	12
Part II Experimental determination of the zero shear radius	
1. Introduction	13
2. Experimental equipment	13
2.1 Atmospheric test rig	13
2.2 Test rods	13
2.3 Traverse device at outlet	14
2.4 Stagnation pressure probe	15
2.5 Hot-wire anemometer	15
2.6 Data recording equipment	15
3. Experimental procedure	16
4. Introductory experiments	16
4.1 Vibration measurements	16
4.2 Velocity distribution at outlet	16
4.3 Control of flow meter and stagnation pressure probe	17

cont.

5.	Evaluation of the data	17
5.1	General	17
5.2	Turbulence measurements	18
6.	Estimation of possible errors	20
6.1	Accuracy of the measurements	20
6.1.1	General	20
6.1.2	Turbulence measurements	21
6.2	Turbulence measurements with the probe slightly inclined to the main flow direction	21
6.3	Effect on the results	22
6.3.1	Effect on friction factor and Reynolds number	23
6.3.2	Effect on turbulence results	23
7.	Measurements in smooth circular channel	23
7.1	Axial and radial turbulence	24
7.2	Shear stress distributions	24
7.3	Conclusions	25
8.	Measurements in annular channel	26
8.1	Experimental results	26
8.2	Analysis of the results	26
9.	Error introduced by use of Hall's [5] theory for separation of friction factors	27
10.	Conclusions	29
11.	Acknowledgements	29
12.	Nomenclature	30
13.	References	32
	Appendix 1	34

Figures

PART I

THEORETICAL CONSIDERATIONS

1. INTRODUCTION

Separation of the shear stresses at the two walls for flow in annular channels has been studied by several investigators, whose main object were to correlate heat transfer and friction in smooth annuli. The problem has gained new interest since the advantages connected with surface roughening of fuel elements in nuclear reactors were realized.

Heat transfer and pressure drop experiments with rough surfaces are very conveniently made in annular geometry with a rough test rod in a smooth shroud. The application of such data to rough rod clusters requires a method for separation of the effects of the two surfaces. A theory for this separation has been submitted by Hall [5]. However, for application of the theory the position of the surface through which the net (time average) transfer of momentum is zero must be known. Hall [5], as well as earlier investigators, assumed that this occurs where the velocity gradient is zero. However, this is not true for turbulent flow in general as has been shown in measurements by Eskinazi [4] in a curved channel, and by Mathieu [8] in a jet impinging on a surface.

It is commonly assumed that the shear stress in turbulent flow can be calculated from:

$$\tau = (\rho \epsilon_M + \eta) \frac{\partial \bar{u}}{\partial r} \quad (I-1)$$

where ϵ_M is the eddy diffusivity of momentum, cf Schlichting [13]. This of course immediately gives equal radii for zero shear and zero velocity gradient. However, as will be shown below, eq. 1 includes some assumptions about the nature of the turbulence, assumptions which cannot immediately be accepted. A more general understanding of the problem can be obtained if the basic equations of the flow are studied.

2. BASIC EQUATIONS

2.1 General equations

In turbulent flow, velocities, fluid properties, pressure and temperature can be separated into a time mean value and a fluctuating component. For instance, the instantaneous value of the axial velocity can be written as:

$$u = \bar{u} + u' \quad (I-2)$$

where the mean value is defined as:

$$\bar{u} = \lim_{t \rightarrow \infty} \frac{1}{t} \int_0^t u \, dt \quad (I-3)$$

The Navier-Stokes equations which are valid if the fluid can be considered as a continuum should apparently also hold for turbulent flow if the motion of the fluid is studied in sufficient detail. If the instantaneous values written as in eq. 2 are put into the Navier-Stokes equations for incompressible, constant viscosity flow written in tensor form and the time mean values are taken, one obtains what are generally known as the Reynolds equations:

$$\rho \left(\frac{\delta \bar{u}_i}{\delta t} + \bar{u}_j \frac{\delta \bar{u}_i}{\delta x_j} \right) = \rho X_i - \frac{\delta \bar{p}}{\delta x_i} + \frac{\delta}{\delta x_j} \left(\eta \frac{\delta \bar{u}_i}{\delta x_j} - \rho \overline{u'_i u'_j} \right) \quad (I-4)$$

The continuity relationships for the mean motion and the fluctuations read:

$$\frac{\delta \bar{u}_i}{\delta x_i} = 0 \quad (I-5)$$

$$\frac{\delta u'_i}{\delta x_i} = 0 \quad (I-6)$$

cf. Rouse [12].

2.2 Transformation to cylindrical coordinates

If cylindrical coordinates are employed, and if the body forces are neglected, equation 4 will give:

$$\begin{aligned} \frac{\delta \bar{u}}{\delta t} + \bar{u} \frac{\delta \bar{u}}{\delta x} + \bar{r} \frac{\delta \bar{u}}{\delta r} + \bar{\varphi} \frac{\delta \bar{u}}{\delta \varphi} = - \frac{1}{\rho} \frac{\delta \bar{p}}{\delta x} + v \nabla^2 \bar{u} - \frac{\delta}{\delta x} \overline{u'^2} - \\ - \frac{1}{r} \frac{\delta}{\delta r} r \overline{u' r'} - \frac{\delta}{\delta \varphi} \overline{u' \varphi'} \end{aligned} \quad (I-7)$$

$$\begin{aligned} \frac{\delta \bar{r}}{\delta t} + \bar{u} \frac{\delta \bar{r}}{\delta x} + \bar{r} \frac{\delta \bar{r}}{\delta r} + \bar{\varphi} \frac{\delta \bar{r}}{\delta \varphi} - r \bar{\varphi}^2 = - \frac{1}{\rho} \frac{\delta \bar{p}}{\delta r} + v (\nabla^2 \bar{r} - \frac{2}{r} \frac{\delta \bar{\varphi}}{\delta \varphi} - \\ - \frac{\bar{r}}{r^2}) - \frac{\delta}{\delta x} \overline{u' r'} - \frac{1}{r} \frac{\delta}{\delta r} r \overline{r'^2} - \frac{\delta}{\delta \varphi} \overline{r' \varphi'} + r \overline{\varphi'^2} \end{aligned} \quad (I-8)$$

$$\begin{aligned} r \frac{\delta \bar{\varphi}}{\delta t} + r \bar{u} \frac{\delta \bar{\varphi}}{\delta x} + \bar{r} \frac{\delta r \bar{\varphi}}{\delta r} + r \bar{\varphi} \frac{\delta \bar{\varphi}}{\delta \varphi} + \bar{r} \bar{\varphi} = - \frac{1}{\rho r} \frac{\delta \bar{p}}{\delta \varphi} + \\ + v (\nabla^2 r \bar{\varphi} + \frac{2}{r^2} \frac{\delta \bar{r}}{\delta \varphi} - \frac{\bar{\varphi}}{r}) - r \frac{\delta}{\delta x} \overline{u' \varphi'} - \frac{\delta}{\delta r} r \overline{r' \varphi'} - \\ - r \frac{\delta}{\delta \varphi} \overline{\varphi'^2} - 2 \overline{r' \varphi'} \end{aligned} \quad (I-9)$$

with

$$\nabla^2 = \frac{\delta^2}{\delta x^2} + \frac{\delta^2}{\delta r^2} + \frac{1}{r} \frac{\delta}{\delta r} + \frac{1}{r^2} \frac{\delta^2}{\delta \varphi^2}$$

Equations 5 and 6 give:

$$\frac{\delta \bar{u}}{\delta x} + \frac{1}{r} \frac{\delta r \bar{r}}{\delta r} + \frac{\delta \bar{\varphi}}{\delta \varphi} = 0 \quad (I-10)$$

$$\frac{\delta u'}{\delta x} + \frac{1}{r} \frac{\delta r r'}{\delta r} + \frac{\delta \varphi'}{\delta \varphi} = 0 \quad (I-11)$$

2.3 Application to steady flow in annuli with constant cross-section area

For steady, incompressible flow in circular and annular channels with constant cross-section area, the following conditions are fulfilled:

- a) All mean quantities are independent of time.
- b) All mean quantities are constant in the circumferential direction and $\bar{\phi} = 0$.
- c) All mean quantities except the pressure are constant in the axial direction.
- d) Boundary conditions:

At the walls, $r = r_1$ and $r = r_2$, all velocities vanish i.e.

$$\bar{u} = \bar{v} = \bar{\phi} = u' = v' = \phi' = 0 \quad (\text{I-12})$$

Condition c is not exactly valid for a channel with rough walls. It will be assumed however that the axial variations are negligible at some distance from the rough wall small in comparison with the channel width, and that the flow further from the wall is approximately the same as that obtained in a smooth channel with the same wall shear stress.

Because of (b) and (c) eq. 10 gives $r \bar{v}$ constant. Since it is zero at the walls it must be zero at all radii.

The Navier-Stokes equations can now be reduced to:

in the axial direction,

$$-\frac{1}{\rho} \frac{\delta \bar{p}}{\delta x} + \frac{1}{r} \frac{\delta}{\delta r} \left(\nu r \frac{\delta \bar{u}}{\delta r} - r \overline{u'v'} \right) = 0 \quad (\text{I-13})$$

in the radial direction,

$$-\frac{1}{\rho} \frac{\delta \bar{p}}{\delta r} - \frac{1}{r} \frac{\delta}{\delta r} r \overline{v'^2} + r \overline{\phi'^2} = 0 \quad (\text{I-14})$$

and in the circumferential direction,

$$- 3 \overline{\dot{r}'} \overline{\dot{\phi}'} - r \frac{\delta \overline{\dot{r}'} \overline{\dot{\phi}'}}{\delta r} = 0 \quad (\text{I-15})$$

Equation 15 can easily be integrated to yield:

$$r^3 \cdot \overline{\dot{r}'} \overline{\dot{\phi}'} = C \quad (\text{I-16})$$

and since $\overline{\dot{r}'} \overline{\dot{\phi}'}$ must be zero at the walls this holds for the entire flow. However, this does not necessarily mean that either \dot{r}' or $\dot{\phi}'$ are zero except at the walls.

Differentiation of eq. 14 with respect to x yields:

$$\frac{\delta}{\delta x} \frac{\delta \overline{p}}{\delta r} = 0 \quad \text{or} \quad \frac{\delta}{\delta r} \frac{\delta \overline{p}}{\delta x} = 0 \quad (\text{I-17})$$

Thus $\frac{\delta \overline{p}}{\delta x}$ is independent of r , a very important result since this makes it possible to measure the axial pressure gradient for incompressible flow with holes in the channel walls. The pressure itself, however, as eq. 14 shows, is not independent of the radial position in turbulent flow.

The energy equation for the mean motion is simply obtained by multiplication of each of the momentum equations with the respective mean velocity in the same direction and adding. Since $\overline{\dot{r}}$ and $\overline{\dot{\phi}}$ both are zero this gives:

$$\overline{u} \left[- \frac{1}{\rho} \frac{\partial \overline{p}}{\partial r} + \frac{1}{r} \frac{\partial}{\partial r} \left(\nu r \frac{\partial \overline{u}}{\partial r} - r \overline{u' \dot{r}'} \right) \right] = 0 \quad (\text{I-18})$$

The energy equation for the fluctuations can be obtained in a similar manner but is of no help in the following discussion since by this single equation 14 additional unknown quantities are introduced.

3. CALCULATION OF THE RADIUS OF ZERO SHEAR

As can be seen from eq. 13 the only remaining shear stress in the axial direction is

$$\tau_{xr} = \eta \frac{\delta \overline{u}}{\delta r} - \rho \overline{u' \dot{r}'} \quad (\text{I-19})$$

Thus the assumption of zero shear where $\frac{\delta \bar{u}}{\delta r} = 0$ is based upon the assumption that $\overline{u' r'} = 0$ where $\frac{\delta \bar{u}}{\delta r} = 0$.

This cannot immediately be accepted for a general case, although of course it must be true for symmetry reasons for some channel geometries, such as a circular tube or parallel plates.

If eq. 19 is compared to eq. 1 it is evident that the eddy diffusivity should be defined as

$$\epsilon_M = - \frac{\overline{u' r'}}{\frac{\partial \bar{u}}{\partial r}} \quad (I-20)$$

Since cases where $\overline{u' r'} \neq 0$ when $\frac{\delta \bar{u}}{\delta r} = 0$ seem possible, the shear stress at the radius of zero velocity gradient must be calculated as

$$\tau_{\hat{r}} = \lim_{r \rightarrow \hat{r}} \left(\epsilon_M \frac{\partial \bar{u}}{\partial r} \right) \quad (I-21)$$

if the eddy diffusivity concept is used.

Integration of eq. 13 gives:

$$- \frac{\delta \bar{p}}{\delta x} \cdot \frac{r^2}{2} + \eta r \frac{\delta \bar{u}}{\delta r} - r \rho \overline{u' r'} + \frac{\delta \bar{p}}{\delta x} \frac{r_0^2}{2} = 0 \quad (I-22)$$

since $\eta \frac{\delta \bar{u}}{\delta r} - \rho \overline{u' r'} = 0$ at the zero shear radius r_0 .

This equation makes it possible to calculate the radial shear stress distribution if r_0 or the total shear stress at some radius is known.

Repeated integration from r_1 to r_2 gives the equation for the zero shear radius:

$$r_0^2 = \frac{r_2^2 - r_1^2 + \frac{4\rho}{\delta \bar{p} / \delta x} \int_{r_1}^{r_2} \overline{u' r'} dr}{2 \ln r_2 / r_1} \quad (I-23)$$

Integration of eq. 22 from r to r_2 gives the velocity distribution,

$$\begin{aligned} \bar{u} = & \frac{1}{2\eta} \frac{\delta \bar{p}}{\delta x} \left[\frac{r^2}{2} - \frac{r_2^2}{2} + \frac{r_2^2 - r_1^2}{2 \ln \frac{r_2}{r_1}} \cdot \ln \frac{r_2}{r} \right] - \\ & - \frac{1}{\nu} \int_r^{r_2} \overline{u' r'} dr + \frac{\ln \frac{r_2}{r}}{\ln \frac{r_2}{r_1}} \cdot \frac{1}{\nu} \cdot \int_{r_1}^{r_2} \overline{u' r'} dr \end{aligned} \quad (I-24)$$

For laminar flow where the integrals vanish, eqs. 23 and 24 reduce to the well known equations for such flow, cf. Knudsen and Katz [6].

In order to calculate the shear stress distribution in the channel (eq. 19), the radial distributions of \bar{u} and $\overline{u'r'}$ must be known. The available equations, namely 10; 11; 13; 14; 16, are not sufficient for this purpose since the number of unknowns exceeds the number of equations. Eq. 18 adds nothing new since it can be reduced immediately to eq. 13.

Consequently it is not possible to calculate theoretically the zero shear radius nor the shear stress at the radius of maximum velocity. It can therefore be concluded that starting from the momentum equations, the continuity relation and the energy equation, it is not possible to show that the radii of zero shear and zero velocity gradient are coincident, except when symmetry conditions can be applied.

4. INTEGRAL ANALYSIS OF THE CONDITIONS AT THE RADIUS OF MAXIMUM VELOCITY

The differential equations show quite definitely that the radii of zero shear and zero velocity gradient may be different, but it is difficult to obtain a real feeling for the problem from these equations. Some additional clarity is obtained by an integral analysis of the flow.

Consider an annular channel (Fig. 1) with a radius of maximum velocity equal to \hat{r} . Divide the channel into two subchannels, one on each side of \hat{r} . The velocity distributions in the subchannels are $u_1(r)$ and $u_2(r)$ respectively.

Assume that fluid lumps are carried from channel 1 to channel 2 and vice versa. From each radial element Δr in channel 1 (per unit length) a fluid transfer $\Delta \dot{m}_{r_{12}}$ to the other channel will occur, and correspondingly a transfer $\Delta \dot{m}_{r_{21}}$ will occur in the opposite direction. It is obvious for continuity reasons that:

$$\int_{r_1}^{\hat{r}} d\dot{m}_{r_{12}} = \int_{\hat{r}}^{r_2} d\dot{m}_{r_{21}} = \dot{m}_r \quad (I-25)$$

The fluid transport from the radial element will give rise to a momentum transport:

$$\Delta I_{12} = \Delta \dot{m}_{r_{12}} \cdot u_{t_1}(r) \quad (I-26)$$

where $u_t(r)$ is the velocity transported across the border between the channels, not necessarily the initial velocity of the fluid lump. Since a similar equation can be written for the momentum transfer from channel 2 to 1, the net transfer across the border will be:

$$I_{12} - I_{21} = \int_{r_1}^{\hat{r}} \dot{m}_{r_{12}} u_{t_1} - \int_{\hat{r}}^{r_2} \dot{m}_{r_{21}} u_{t_2} \quad (I-27)$$

This momentum transfer is equivalent to a shear stress:

$$\hat{\tau} = - \frac{1}{\pi \hat{r}} (I_{12} - I_{21}) \quad (I-28)$$

which, utilizing eqs 25 and 27, can be written:

$$\hat{\tau} = - \frac{\dot{m}_r}{\pi \hat{r}} \left[\frac{\int_{r_1}^{\hat{r}} \dot{m}_{r_{12}} u_{t_1}}{\int_{r_1}^{\hat{r}} \dot{m}_{r_{12}}} - \frac{\int_{\hat{r}}^{r_2} \dot{m}_{r_{21}} u_{t_2}}{\int_{\hat{r}}^{r_2} \dot{m}_{r_{21}}} \right] \quad (I-29)$$

With properly chosen mean values this reduces to:

$$\hat{\tau} = - \frac{\dot{m}_r}{\pi \hat{r}} (\bar{u}_{t_1} - \bar{u}_{t_2}) \quad (I-30)$$

Four cases where this shear stress is zero can now be distinguished.

- a) $\dot{m}_r = 0$
- b) $u_{t_1} \equiv u_{t_2}$

This will generally occur only in cases of perfect symmetry such as in circular channels and parallel plate channels.

- c) The transport path of the fluid lumps is so small that differences

between \bar{u}_{t_1} and \bar{u}_{t_2} will not occur even if the velocity distributions in the two subchannels are quite different.

d) The characteristics of the flow are such that $\bar{u}_{t_1} = \bar{u}_{t_2}$ even if the velocity distributions are different.

The analysis is obviously valid for both laminar and turbulent flow, with the only difference that in laminar flow the fluid lumps consist of single molecules, in turbulent flow of agglomerates of fluid.

Conditions a and c will obviously only be fulfilled in the same approximation as the assumption that the fluid is continuous and traveling only in the axial direction, i. e. what is normally assumed for laminar flow and in simple treatments of turbulent flow. This may be taken to mean that the distance between the zero shear surface and the surface of maximum velocity will be of the same order of magnitude as the free path length of the fluid lumps. Under normal conditions the distance would be quite negligible for laminar flow but important for turbulent flow where in the middle of a channel the free path length is of the order of 10 % of the channel width.

Except under condition b, the shear stress is zero at the radius of maximum velocity in turbulent flow only when condition d is valid.

It is obvious that the validity of condition d cannot be judged without detailed information about the turbulent flow, information which is not available.

The conclusion is therefore the same as earlier. The radii of zero shear and zero velocity gradient are not necessarily coincident for turbulent flow in annuli.

5. CONCLUSIONS FROM THE THEORETICAL CONSIDERATIONS

- a) Theoretical calculation of the shear stress distribution for turbulent flow in annuli is not possible.
- b) It is not evident that the radii of zero shear and zero velocity gradient coincide.
- c) Once the zero shear radius or the shear stress at some radius is known, the shear stress distribution can be calculated if the axial pressure gradient is given. Experiments are necessary for this.

6. NOMENCLATURE

I	momentum
m	mass
\dot{m}	mass flow
p	pressure
r	radius
\dot{r}	radial velocity
t	time
u	velocity in x-direction
v	" " y- "
w	" " z- "
x	axial coordinate
y	coordinate
z	coordinate
ϵ	eddy diffusivity
η	dyn. viscosity
ν	kinematic viscosity $\nu = \eta/\rho$
ρ	density
τ	shear stress
φ	angular coordinate
$\dot{\varphi}$	angular velocity

Subscripts:

0	zero shear surface
1	inner surface or inner subchannel
2	outer surface or outer subchannel
r	radial/unit length
r_{12}	radially from subchannel 1 to 2/unit length
r_{21}	radially from subchannel 2 to 1/unit length
t	transferred

Special signs:

'	fluctuating component, for instance u'
$\bar{\quad}$	mean value
\wedge	surface of maximum velocity

PART II

EXPERIMENTAL DETERMINATION OF THE ZERO SHEAR RADIUS

1. INTRODUCTION

It was concluded from the theoretical analysis in part I that experimental determination of the zero shear radius or the shear stress at some radius is necessary for calculation of the shear stress distribution in an annulus.

Results of such measurements are given below. It is not claimed that this experimental investigation is exhaustive; the aim of it was only to check if the difference between the radii of zero shear and zero velocity gradient is large enough to be practical interest.

2. EXPERIMENTAL EQUIPMENT

2.1 Atmospheric test rig

The experiments were performed in the outlet of an atmospheric air rig, Fig. 2.

Air was drawn from outside the building through a filter by the compressor which blew it through a flow straightener, a flow rate meter, a contraction section, and finally through the test section consisting of a circular tube, i.d. 130.05 mm, length 3890 mm, honed inside.

Smooth or roughened test rods could be positioned in the test channel. The centricity was ensured by radial struts at the middle of the rods and by thin (diam. 0.5 mm) wires at the outlet, Fig. 4.

The rig was provided with a calibrated Foster flow meter (cf ref. [15]), probes for measurement of inlet pressure and temperature, and static pressure holes, (diam. 0.7 mm) four at each axial position, for measurement of the axial pressure gradient.

2.2 Test rods

One smooth and two roughened rods were tested. The diameter of the smooth rod and the root diameter of the rough rods was 29.0 mm. The roughness consisted of two-dimensional fins. The dimensions and shapes of these were checked using a shadow projector (SIP-projector, kindly placed at our disposal by AB Stal-Laval, Nacka) where magnifications up to 50 times could be obtained.

A transparent paper was placed on the ground glass plate and shadowgraphs were taken along two opposite sides of the test rod at each 100 mm from 500 to 1500 mm from the outlet end. The magnification was chosen so that at least three fins were shown on each shadowgraph. The dimensions were then measured from the drawings. Mean values for the height, the pitch-to-height ratio and pitch-to-width ratio were calculated, together with the standard deviations from the mean values.

The measured fin-dimensions are given in Fig. 29 together with representative examples of the shadowgraphs. These illustrations have been reduced from the original size.

2.3 Traverse device at outlet

The traverse device used for the velocity and turbulence measurements is shown in Fig. 3. It consisted of a milling machine table, movable in two orthogonal directions by precision screws, one turn corresponding to 5 mm displacement of the table. The displacement was measured on scales graduated in 0.05 mm showing the rotation of the screws.

The probe support was mounted on this table. Two different designs were used. The original design, Fig. 4A, used in the annulus experiments and the first set of measurements in a circular channel, consisted of a support head designed to make rotation of the probe around its own axis possible, and two struts, one of which contained the axis for control of the probe rotation.

However, it became evident that rotation of the probe was not an accurate way of measuring the shear stress with a slanting wire probe, since the straightness of the probes was not sufficient. Traversing first with one slanting angle, then, after adjusting scales as explained below, with the probe rotated 180° was then considered far better.

The probe support was then modified, the support head being made more slender for less disturbance of the flow. The modified design, Fig. 4B, used in the later measurements in a circular channel consisted of a slender support head (diam. 8 mm), fixed by four streamlined radial struts with a maximum thickness of 4 mm to a ring with a diameter sufficiently large not to disturb the flow. The ring was fixed to the table of the traverse device.

Before the experiments, the table was carefully adjusted so that the channel axis was normal to the table plane and parallel to the probe support axis. However, owing to the slenderness of the miniature hot-wire probes it was not possible to ensure that they were exactly parallel to the channel axis. This is discussed further in section 6.2.

During measurements the distance between the probe tip and the support head was about 135 mm.

Since the probes used were very slender and they could not be made sufficiently straight, a special device was used for the zero adjustment of the screw scales. It consisted of a magnifying tube with an engraved scale. The coordinates of the point in the channel corresponding to the zero value of the scale and best sharpness of the picture being known, it was possible to move the probe tip into this position and adjust the scales. By this method the tip position could be determined within less than 0.02 mm in the main traversal direction (y) and within 0.1 mm in the normal direction (z).

2.4 Stagnation pressure probe

The stagnation pressure probe consisted of a thin-walled stainless steel tube (diam. 1.0 mm) which was mounted in the probe support, with its axis parallel to the flow direction.

2.5 Hot-wire anemometer

A constant temperature anemometer, DISA 55 A 01, with miniature probes (tip diam. 2 mm) were used - 55 A 25 with the wire normal to the main flow or 55 A 29 with the wire at about 45° to the main flow. The technical data for the anemometer are given in data sheets supplied by DISA Elektronik A/S, Herlev, Denmark.

2.6 Data recording equipment

All measurements except those made with the anemometer were made with a 4-figure digital voltmeter, after transformation of all quantities to voltages, utilizing thermocouples, pressure transducers etc. The data were registered on punched tape as explained in the description of the FRIGGA III rig (ref. [15]).

3. EXPERIMENTAL PROCEDURE

After calibration of the pressure transducers against Betz micro-manometers the blower was started and steady state conditions awaited. Pressures, temperatures and pressure drops in the test section were then registered twice by the data recorder, after which a stagnation pressure traverse was made across the channel 35 mm down from the outlet. Except for some of the introductory experiments (section 4.2) traverses were made only in the y direction, though always at both sides of the center. After preparation of the anemometer according to the manual, hot-wire traverses were made, similar to the stagnation pressure traverse. Measurements were made on both sides of the center with the wire normal to the flow and at yaw angles $\sim \pm 45^\circ$, traversing first at the + value, then at the - value.

Stagnation pressure readings were made at each 5 mm in the circular tube tests and at each 1.25 mm in the annulus tests, whereas turbulence measurements were made at each 5 and 2.5 mm respectively.

After the hot-wire traverses a repetition of the stagnation pressure traverse was made, followed by two registrations of all pressures, temperatures, etc.

The hot wires were run at about 250°C , the air temperature being $50\text{-}70^\circ\text{C}$.

4. INTRODUCTORY EXPERIMENTS

4.1 Vibration measurements

Since vibrations of the test section and the probe support cannot be separated from the turbulence, they must be kept as small as possible.

Measurements by Rolandsson [11] showed amplitudes below 0.01 mm at frequencies of 50-80 Hz for velocities below 100 m/s, which was accepted.

4.2 Velocity distribution at outlet

Velocity distributions were measured at 0, 35 and 70 mm below the outlet. No significant differences could be found, and it was decided to perform the main measurements at 35 mm below the outlet.

The flow distribution there was checked by traversing in the y and z directions. The differences were below 3 % for the velocity, as is illustrated by Figs. 5 and 6 showing the stagnation pressure distributions for the smooth rod experiments.

The differences were probably due to the different disturbances caused by the probe support. They are small enough to be neglected, however.

4.3 Control of flow meter and stagnation pressure probe

To cross-check the flow meter and the velocity traverses, the measured velocity distribution was integrated for the circular tube experiments and compared with the mean velocity calculated from the flow meter.

The agreement was excellent, as is shown in the table below.

Table 4.3.1 Comparison of mean velocities

Exp.no.	Mean velocity from traverses	Mean velocity according to flow meter
5008	40.2 m/s	39.7 m/s
5013	64.0	63.7
5153	87.5	86.2

5. EVALUATION OF THE DATA

5.1 General

The evaluation was performed on the Ferranti Mercury Computer.

The equations for air data obtained from NBS tables [16] given in ref. [14] were utilized, as well as the equations from ref. [14] for calculation of temperatures from thermocouple emf's and the mass flow from temperature and pressure readings. Gas properties were evaluated at static pressure and temperature.

The Reynolds number was calculated from

$$Re = \frac{4\dot{m}}{\eta U} \quad (\text{II-1})$$

U being the "wetted" perimeter for the channel.

The friction pressure drop was calculated from the measured pressure difference by deduction of the acceleration pressure drop:

$$\Delta p_f = \Delta p_{msd} - \frac{\dot{m}}{A} \cdot \Delta \bar{u} \quad (\text{II-2})$$

The friction factor was then obtained from

$$f = \frac{\Delta p_f}{\Delta x} \cdot \frac{8 A^3}{U} \frac{\rho}{\dot{m}^2} \quad (\text{II-3})$$

The velocities at the outlet were calculated from:

$$\bar{u} = \sqrt{\frac{2(p_{tot} - p_{stat})}{\rho}} \quad (\text{II-4})$$

where p_{tot} is the mean value of the readings at the same radius on the two sides of the center.

The laminar shear stress was obtained from

$$\tau_l = \eta \frac{\delta u}{\delta r} \quad (\text{II-5})$$

with the velocity gradient at the i th point of measurement calculated as:

$$\left(\frac{\delta u}{\delta r}\right)_i = \frac{8(\bar{u}_{i+1} - \bar{u}_{i-1}) - u_{i+2} + u_{i-2}}{12 \Delta r} \quad (\text{II-6})$$

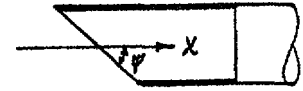
5.2 Turbulence measurements

The equations for calculation of the turbulent velocity fluctuations from the mean voltage and RMS readings on a constant current hot wire anemometer have been derived by Patel [10].

It is assumed that the wire is cooled only by the velocity component perpendicular to the wire and that the equation governing the voltage reads:

$$\frac{V^2}{R} = a + b (u \sin \Psi)^c (R - R_a) \quad (\text{II-7})$$

Differentiation and assumption of small velocity fluctuations in comparison with the mean velocity gives:



$$\left(\frac{2V}{V^2 - V_0^2}\right) dV = \frac{c}{u} (u' + r' \cot \Psi) \quad (\text{II-8})$$

The time mean value is taken after squaring the equation:

$$\left(\frac{2V}{V^2 - V_0^2}\right)^2 \cdot \overline{V'^2} = \frac{c^2}{\overline{u^2}} (\overline{u'^2} + \overline{r'^2} \cot^2 \Psi + 2\overline{u'r'} \cot \Psi) \quad (\text{II-9})$$

Using a normal wire with $\Psi=90^\circ$ gives the axial turbulence;

$$\overline{u'^2} = \frac{\overline{u^2}}{c^2} \cdot \left(\frac{2V}{V^2 - V_0^2}\right)^2 \cdot \overline{V'^2} \quad (\text{II-10})$$

whereas two measurements with a slanting wire $\Psi = \Psi$ and $180-\Psi$ gives the radial turbulence after adding the two equations II-9 and utilizing the value found for $\overline{u'^2}$ in eq. II-10:

$$\overline{r'^2} = \tan^2 \Psi \left[\frac{\overline{u^2}}{2c^2} (\beta^2_{(+)} \overline{V'^2}_{(+)} + \beta^2_{(-)} \overline{V'^2}_{(-)}) - \overline{u'^2} \right] \quad (\text{II-11})$$

where

$$\beta = \frac{2V}{V^2 - V_0^2} \quad (\text{II-12})$$

The turbulent shear stress $-\rho \overline{u'r'}$, which according to eqs. 1-19 is the only one acting in the axial direction, is obtained from the same measurements by subtracting the two equations II-9:

$$-\rho \overline{u'r'} = \frac{\rho \overline{u^2} \tan \Psi}{4c^2} (\beta^2_{(-)} \overline{V'^2}_{(-)} - \beta^2_{(+)} \overline{V'^2}_{(+)}) \quad (\text{II-13})$$

The voltages V , V_0 and $\sqrt{\overline{V'^2}}$ were measured with the instruments on the anemometer, and the calculations were performed with the mean values for the two readings at the same radius, taking into ac-

count that for the slanting wire measurements the (+) values on one side correspond to (-) values on the other.

The velocities \bar{u} were obtained from the velocity traverses.

The yaw angle Ψ for the slanting wire probes was measured in a microscope and found close to, ($\pm 1^\circ$), 45° for all the probes used. Due to the uncertainty of the direction of the probe mentioned earlier (section 2.2) the actual yaw angle will be slightly different. This is discussed further in section 6.2.

The constant c in eq. II-7 requires some discussion. Patel [10] used a value $c=0.45$ and obtained good agreement between measured and theoretical stress distributions for two experiments in a circular tube.

Since eq. II-13 can be written

$$(V^2 - V_o^2) = B \cdot \bar{u}^c \quad (\text{II-14})$$

the constant c can be obtained as the inclination of the straight line

$$\ln(V^2 - V_o^2) = \ln B + c \cdot \ln \bar{u} \quad (\text{II-15})$$

Plotting $\ln(V^2 - V_o^2)$ against $\ln \bar{u}$ for all the measurements gave values of c which differed considerably from 0.45 even if the mean values happened to be 0.444 for the normal wire and 0.449 for the slanting wire runs. This is shown in Figs. 7-11.

Instead of using the mean value, it was preferred to use the value of c determined for each run, given in the figures mentioned.

6. ESTIMATION OF POSSIBLE ERRORS

6.1 Accuracy of the measurements

6.1.1 General

The estimated uncertainties of the measurements are given in the table below.

Pressure measurements

Static and stagnation pressures before and in test section	$\pm 0.25 \%$
Stagnation pressure measured by traversing probe (except close to the walls)	$\pm 0.5 \%$
Axial pressure drop (careful cali- bration close to working point)	$\pm 0.1 \%$

Temperature measurements

All temperatures ($^{\circ}\text{C}$)	$\pm 0.75 \%$
---	---------------

Mass flow measurements

The flow meter had been cali- brated earlier (ref. [15]) and the estimated uncertainty was	$\pm 2 \%$
--	------------

The introductory experiments show
that this still holds (section 4.3)

6.1.2 Turbulence measurements

The direct current voltage could be measured within $\pm 0.5 \%$.

The accuracy of the RMS measurements of the fluctuating com-
ponent is more difficult to estimate. The accuracy of the instrument
permits measurements within $\pm 1.0 \%$. It was observed, however, that
irregular variations of the RMS value with a period of about a minute
occurred. Taking this into account, the uncertainty of the RMS meas-
urements were estimated to be

$$\sqrt{\overline{V'^2}} > 75 \text{ mV} \quad \pm 2.5 \%$$

$$\sqrt{\overline{V'^2}} < 75 \text{ mV} \quad \pm 1.5 \%$$

6.2 Turbulence measurements with the probe slightly
inclined to the main flow direction

As already mentioned, the probes and to some extent the probe

supports were not rigid enough to ensure that the probe axis and the main flow direction were parallel during operation, though the probe support had been carefully adjusted in advance.

Assume that the probe axis is inclined at a small angle Δ to the flow direction. This is illustrated in Fig. 12. The actual yaw angle of the wire will be $\Psi - \Delta$ or $180 - (\Psi + \Delta)$ when the probe is rotated, instead of Ψ and $180 - \Psi$. This uncertainty can almost be eliminated if, as was done in these experiments, measurements are made on both sides of the center of a circularly symmetric channel, including rotation of the probe.

As shown in Fig. 12, the yaw angles for measurements on opposite sides with the probe in the same position relative to the probe support will be the same but with opposite signs. Thus eqs. 11 and 13 can be used if the actual yaw angle ($\Psi - \Delta$) is used instead of the ideal value. If Δ is unknown, eq. 13 can still be used for calculation of the zero shear radius, since the uncertainty only influences the constant before the difference within the brackets.

If measurements are also performed with the probe rotated 180° on the support, and mean values are taken of the corresponding measurements on each side, these mean values will be approximately valid for the ideal yaw angle Ψ , since

$$\tan \Psi = \frac{1}{2} [\tan(\Psi + \Delta) + \tan(\Psi - \Delta)] - \Psi \cdot \Delta^2 + \dots \quad (\text{II-16})$$

and

$$\Psi \cdot \Delta^2 \sim \frac{\pi^2}{180^2} \cdot 45 \cdot 1^2 = 0.24 \cdot 10^{-3}$$

i.e. about 0.2 o/oo of $\tan \Psi$, for $\Delta = 1^\circ$.

Thus, assuming the deviation Δ to be constant, the uncertainty can be almost eliminated this way. However, since variations of Δ with the probe position are possible, a means of checking the actual yaw angle during operation would be very valuable.

6.3 Effect on the results

The uncertainty σ_y of a quantity y which is calculated from independent measured quantities x_i with the uncertainties σ_i can be calculated from

$$\sigma_y = \sqrt{\sum (\sigma_i \frac{\delta f}{\delta x_i})^2} \quad (\text{II-17})$$

when

$$y = f(x_1, x_2, \dots, x_i) \quad (\text{II-18})$$

The uncertainty of a mean value \bar{x} obtained from a number, n , of measurements

$$\bar{x} = \frac{\sum x}{n} \quad (\text{II-19})$$

will be

$$\sigma_{\bar{x}} = \frac{\sigma_x}{\sqrt{n}} \quad (\text{II-20})$$

6.3.1 Effect on friction factor and Reynolds number

Using eqs. 1, 3, 17 and the data in section 6.1.1, the uncertainty of the Reynolds number is found to be $\pm 2.2 \%$ and of the friction factor $\pm 4.1 \%$.

6.3.2 Effect on turbulence results

Assuming that the constant c can be determined within $\pm 3 \%$ from diagrams 7-11, the axial turbulence will be obtained within $\pm 7.2 \%$ (eq. 10).

Assuming further that the value of $\tan \Psi$ can be determined within $\pm 1 \%$ by the measurements in the microscope, the uncertainty of the radial turbulence will be $\pm 10 \%$ and of the turbulent shear stress $\pm 15 \%$ (eqs. 11, 12, 13).

However, the discussion above assumes that the theory for calculation of the turbulence terms from the readings on the anemometer is correct. In order to check this and the experimental technique, measurements were made in a smooth circular channel as described below.

7. MEASUREMENTS IN SMOOTH CIRCULAR CHANNEL

The measurements were made in the rig with the test rod removed.

7.1 Axial and radial turbulence

The measured distributions of axial and radial turbulence compared with the results of Laufer [7] are shown in Figs. 14 and 15.

The agreement is fairly good if the results for the same value of the Reynolds number are compared. The marked effect of the Reynolds number was not observed by Laufer [7], whose curves for $Re = 5 \cdot 10^4$ and $5 \cdot 10^5$ are very close. With this taken into consideration, the agreement seems less good.

No significant difference between the results for the two probe supports can be found.

7.2 Shear stress distributions

It was proved in part I that the axial pressure gradient is independent of the radius for incompressible, axisymmetric flow. Utilizing this, it is possible to calculate the shear stress distribution in a circular channel. A force balance immediately gives:

$$\tau = \frac{r}{2} \frac{\partial p}{\partial x} \quad (\text{II-21})$$

or using the shear stress at the wall:

$$\tau/\tau_2 = r/r_2 \quad (\text{II-22})$$

Since τ_2 is easily calculated from eq. 21, it is possible to check the measured shear stress distribution against the theoretical, if the axial pressure gradient is known.

The comparison is made in Fig. 16, where the measured shear stress has been obtained from:

$$\tau = \eta \frac{\partial \bar{u}}{\partial r} - \rho \overline{u' r'} \quad (\text{II-23})$$

cf. eq. I-19.

The agreement is moderately good but slightly better for the measurements with the modified probe support. Also here a definite dependence on the Reynolds number can be observed. There is further a clear trend for the measured shear stress distributions to be curved, with too high

values close to the wall and too low values in the center region. The same effect may be observed in Patel's [10] measurements.

A check of the measured pressure drops can be obtained by comparison with the data of Nikuradse [9], Fig. 13. The agreement is very good.

7.3 Conclusions

From the comparisons of the results from the measurements in the circular channel, it must be concluded that the results are less accurate than estimated above (6.3.2). For the shear stress measurements, where the correct distribution is known, this is quite evident, the error being up to 50 % in the center region.

In the case of the turbulence components the correct distributions are not exactly known. However, the discrepancies with respect to Laufer's [7] results are discouraging.

It seems obvious that the errors are systematic, since the scatter of the points is small. There can be three main reasons for such errors in this case:

- a) The instrument is faulty.
- b) The handling of the equipment is not correct.
- c) The evaluation of the measured data is not correct.

To improve the technique a better probe support was tried. The results were not very much improved. It is not believed that the error can be eliminated by improving the technique still more, even if some improvements are possible, cf. 6.2. It is suspected that the error is caused by one of the following effects:

- a) Eq. 7 is not valid for the miniature probes used in the experiments ¹⁾.
- b) The linear theory (section 5.2) is not accurate enough for evaluation of the data.

¹⁾ According to a recently published work by FH Champagne (cf. appendix 1), which was noticed first when this report was in the printing stage the direction sensitivity assumed in eq. 7 is true only as an approximation. This does not effect the determination of the zero shear radius as pointed out in appendix 1.

Whichever of these is the reason for the error, it seems reasonable to assume that the error in the shear stress comes in as a multiplicative factor. This means that even if the absolute values of the shear stresses are not correctly measured, the radius of zero shear will be found rather accurately. This is also supported by the results given in Fig. 16.

The measurements in annuli were therefore concentrated on direct determination of the zero shear radius, rather than on measurement of one shear stress and relying on eq. I-21 for calculation of the zero shear radius.

8. MEASUREMENTS IN ANNULAR CHANNEL

8.1 Experimental results

The measured velocity and shear stress distributions are given in Figs 17-27. From these diagrams the zero shear radius could easily be obtained by interpolation. The radius of maximum velocity was obtained from plots of the velocity gradient, calculated from the measured velocities by eq. 6. An example of such a plot is given in Fig. 28.

The measured friction factors are given in Fig. 13.

8.2 Analysis of the results

A single sided t-test was applied to determine whether the experiments did show any significant difference between the radii of zero shear and zero velocity gradient. The different experiments for each rod were treated as repetitions of a single experiment, the influence of the Reynolds number being neglected.

The data are given in Table 8.2.1. As can be seen, the difference is not significant for the smooth rod, in agreement with the findings of Brighton and Jones [1], is significant for the T rod, and almost significant for the F rod. Most probably the difference would have been significant also for the F rod if one of the experiments had not by accident been missing.

Table 8.2.1 Comparison between \hat{r} and r_o

Test rod	$10^{-5} Re$	$\frac{r_2 - \hat{r}}{r_2 - r_1}$	\hat{r} mm	$\frac{r_2 - r_o}{r_2 - r_1}$	r_o mm	$r_o - \hat{r}$ mm	$(\frac{r_o - \hat{r}}{r_o - r_1})$ mm	σ mm	t
A smooth	1.62	0.535	45.74	0.540	45.56	-0.18			
	2.60	0.540	45.55	0.540	45.56	+0.01	-0.192*	0.141	0.272
	2.87	0.542	45.50	0.550	45.20	-0.30			
	3.94	0.542	45.50	0.550	45.20	-0.30			
F	1.58	0.278	55.0	0.245	56.18	+1.18			
	2.09	0.311	53.8	0.240	56.36	+2.56	+1.473**	0.97	2.63
	2.97	0.239	56.4	0.220	57.08	+0.68			
T	1.57	0.369	51.72	0.355	52.22	+0.50			
	2.10	0.369	51.72	0.340	52.76	+1.04	+1.080***	0.425	5.08
	2.89	0.361	52.00	0.325	53.30	+1.30			
	3.87	0.361	52.00	0.320	53.48	+1.48			

* not significant

** almost significant $0.90 > P > 0.95$

*** highly significant $0.99 > P > 0.995$

cf. Davies [3]

9. ERROR INTRODUCED BY USE OF HALL'S [5] THEORY FOR SEPARATION OF FRICTION FACTORS

Assuming the radii of zero shear and zero velocity gradient equal, Hall [5] derived the following formulas for calculation of the friction factors in the two subchannels on either side of the zero shear section in an annulus, if the overall friction factor is known:

$$\hat{f}_1 = f \frac{\hat{r}^2 - r_1^2}{r_2^2 - r_1^2} \cdot \frac{r_2 + r_1}{r_1} \cdot \frac{\overline{\rho u^2}}{\rho_1 \overline{u_1^2}} \quad (\text{II-30})$$

$$\hat{f}_2 = f \frac{r_2^2 - \hat{r}^2}{r_2^2 - r_1^2} \cdot \frac{r_2 + r_1}{r_2} \cdot \frac{\overline{\rho u^2}}{\rho_1 \overline{u_1^2}} \quad (\text{II-31})$$

If $r_0 \neq \hat{r}$ the correct friction factors will be different by a factor:

$$f_{10}/\hat{f}_1 = \frac{r_0^2 - r_1^2}{\hat{r}^2 - r_1^2} \cdot \left(\frac{\hat{\rho} \hat{u}_2}{\rho_0 u_0^2} \right)_1 \quad (\text{II-32})$$

$$f_{20}/\hat{f}_2 = \frac{r_2^2 - r_0^2}{r_2^2 - \hat{r}^2} \cdot \left(\frac{\hat{\rho} \hat{u}_2}{\rho_0 u_0^2} \right)_2 \quad (\text{II-33})$$

The values of these correction factors have been estimated, using for each rod the mean values for \hat{r} and r_0 and calculating the mean velocities for one test with each rough rod.

The results are given in Table 9.1.

Table 9.1 Error introduced by Hall's [5] theory

Test rod	F	T
$\frac{f_{10}}{\hat{f}_1}$	1.037	1.042
$\frac{f_{20}}{\hat{f}_2}$	0.922	0.963

As can be seen, the friction factors on the rough side will be too low, on the smooth side too high, if calculated by Hall's method. This is in agreement with the results of Cowin et al. [2], who made measurements in a rectangular channel roughened on one side or both sides.

In the two cases tested here, the area and velocity terms are acting in different directions, and the resulting correction factors for the inner channel, which is of most practical interest, are close enough to unity to be neglected. This may of course not be generally true. Cowin's [2] results, however, also show that the error is of the order of 10 % or less.

10. CONCLUSIONS

It can be concluded that:

- a) It has been shown by experiments that in the Reynolds number range $10^5 - 4 \cdot 10^5$ and in an annulus with diameter ratio 2.24, the radius of zero shear is equal to the radius of zero velocity gradient for a smooth inner surface, and slightly higher for rough inner surface.
- b) This explains the breakdown of Hall's [5] transformation theory reported by Cowin [2].
- c) The error introduced by using Hall's transformation can be expected to be of the order of 10 % or less.

11. ACKNOWLEDGEMENTS

The authors wish to express their gratitude to Mr. Jan Flinta, Head of the section for experimental heat transfer and mechanics studies, for many valuable discussions, to Mr. Bror Hedberg for his skilful work in making and assembling the test equipment, and for help during the experiments, to Mr. Rolf Lindh who made the computer program for evaluation of the data, and to miss Kerstin Niblaeus who was helpful with plotting of the results.

12. NOMENCLATURE

A	flow area
b	fin width
c	exponent in Collis' law
f	friction factor
h	fin height
\dot{m}	mass flow
p	pressure
Δp	pressure difference
R	electric resistance
r	radius
\dot{r}	radial velocity
Re	Reynolds number
s	fin pitch
t	statistic quantity $t = \frac{\text{mean value}}{\text{standard error of mean}}$
U	perimeter
u	axial velocity
u^+	friction velocity $u^+ = \sqrt{\frac{\tau_w}{\rho}}$
Δu	velocity difference
V	voltage
V_0	voltage at zero velocity
x	axial coordinate
β	defined in eq. II-18
Δ	inclination of probe axis
η	dynamic viscosity
ρ	density
σ	standard deviation
τ	shear stress
Ψ	angle of slanting wire

Subscripts

0	zero shear surface or in case of V_0 zero velocity
1	inner surface or inner subchannel
2	outer " or outer "
a	ambient temperature

+ slanting angle ψ
- " " $180 - \psi$
dyn dynamic
f friction
 l laminar
msd measured
stat static
tot total
w wall

Special signs

' fluctuating, example u'
— mean value, example \bar{u}
^ maximum velocity

13. REFERENCES

1. BRIGHTON, J A and JONES, J B,
Fully developed turbulent flow in annuli.
Journ. Basic Engineering 86 (1964) 835-44.
2. COWIN, M, WILKIE, D et al.,
Friction factor measurements in a rectangular channel with
artificially roughened walls. 1963.
(TRG rep. 539 (W) .)
3. DAVIES, O L, (ed.)
The design and analysis of industrial experiments. 2 ed. rev.
London, Hafner Pub. 1960.
4. ESKINAZI, S and YEH, H,
An investigation on fully developed flows in curved channels.
Journ. Aeronaut. Sci. 23 (1956) 23-34.
5. HALL, W B,
Heat transfer in channels composed of rough and smooth
surfaces. 1958.
(IGR - TN/W - 832.)
6. KNUDSEN, J G and KATZ, D L,
Fluid dynamics and heat transfer.
New York, Mc Graw 1958.
7. LAUFER, J,
The structure of turbulence in fully developed pipe flow. 1953.
(NACA rep. 1174.)
8. MATHIEU, J,
Contribution à l'étude aérothermique d'un jet plan évoluant
en présence d'une paroi. Paris 1961.
(Publ. Scient. et Techn. du Ministère de l'air. No 374.)
9. NIKURADSE, J,
Gesetzmässigkeiten der turbulenten Strömung in glatten Röhren. 1932.
(VDI Forsch. -heft 356.)
10. PATEL, R P,
Measurements of the Reynolds stresses in a circular pipe as a
means of testing a DISA constant-temperature hot-wire ane-
mometer. 1963.
(McGill University Montreal T-N-63-6.)
11. ROLANDSSON, S,
Bestämning av vibrationer i FRIGGA V. 1965.
AB Atomenergi, Sweden (Internal report AP-RTL-5537) (In Swedish).
12. ROUSE, H, (ed.)
Advanced mechanics of fluids.
New York, Wiley 1959.

13. SCHLICHTING, H,
Boundary layer theory. 4 ed.
New York, Mc Graw 1960.
14. KJELLSTRÖM, B, LARSSON, A and LINDH, R,
Studies of heat transfer and pressure drop for flow of air in an
annular channel with roughened inner surface.
- Evaluation of experimental data. 1. 1964.
AB Atomenergi, Sweden (Internal report RPL-665).
15. KJELLSTRÖM, B and LARSSON, A,
The atmospheric heat transfer rig FRIGGA III. 1964.
AB Atomenergi, Sweden (Internal report RPL-733).
16. Tables of thermal properties of gases. Wash. 1955.
(NBS Circ. 564.)

APPENDIX I

Recent findings about the direction sensitivity of hot-wires

F H Champagne in a recently published work "Turbulence measurements with inclined hot-wires" (Ph. D. Thesis - Washington Univ. Dec. 1965) D1-82-0491, which is only known to the author in the form of an abstract, STAR (4) 10, May 23, 1966, N66-20202, states that the direction sensitivity does not follow the simple sine-law as assumed in eq. II-7 and that a better correlation is obtained by:

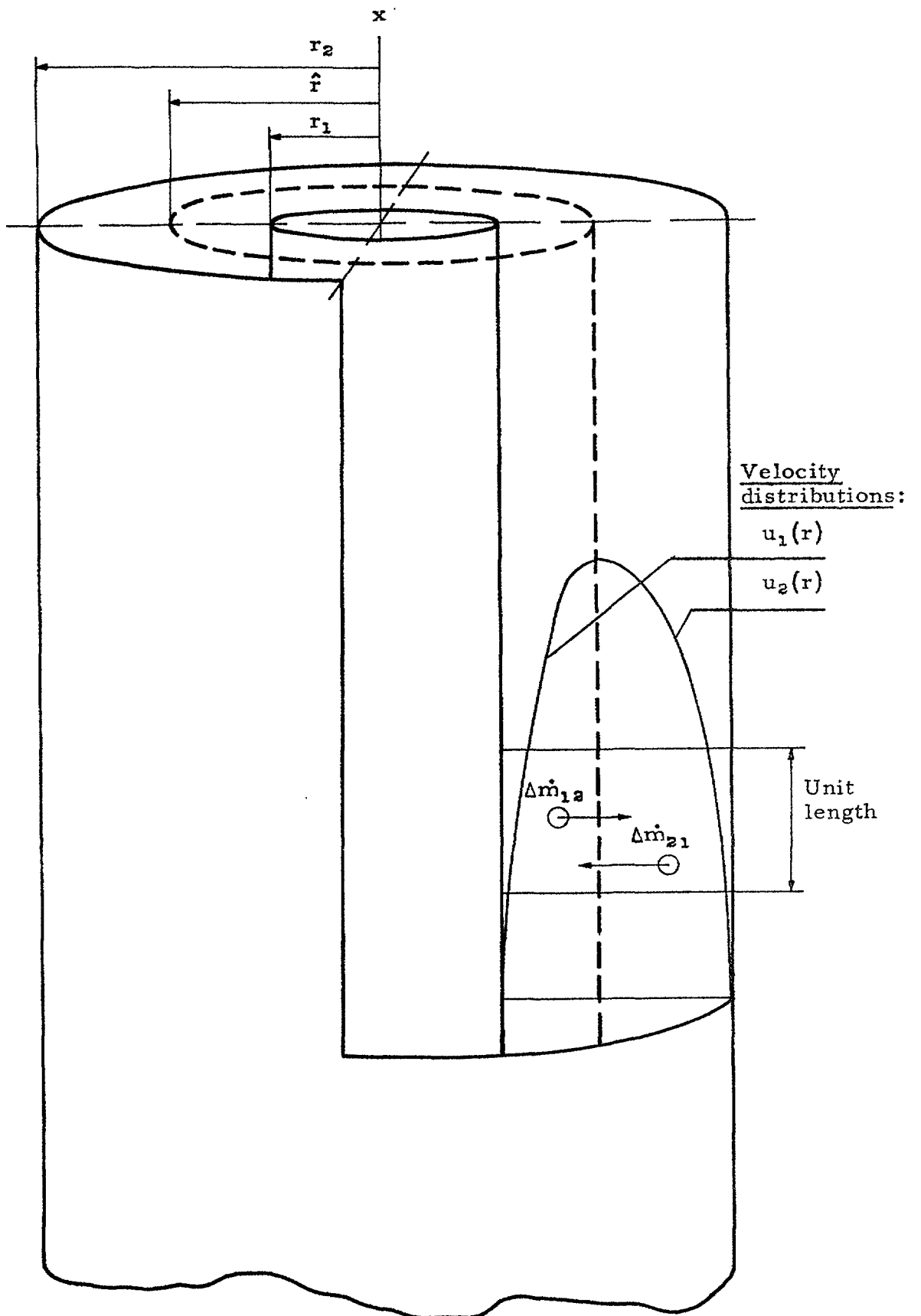
$$u^2(\Psi) = u^2(0) \cdot (\sin^2 \Psi + k^2 \cos^2 \Psi) \quad (1-1)$$

where k is dependent mainly of the length to diameter ratio of the wire. If this is introduced in eq. II-7 and the operations leading to eq. II-13 are carried through, the shear stress will be obtained as:

$$-\rho \overline{u' \dot{r}'} = \frac{\rho \overline{u^2}}{4c^2} \cdot \frac{\tan \Psi + k^2 \cot \Psi}{1 - k^2} \left[\beta^2(-) \overline{V'^2(-)} - \beta^2(+)\overline{V'^2(+)} \right] \quad (1-2)$$

Comparison of eqs. II-13 and 2 above shows that the difference is the factor before the brackets.

The zero shear radius is therefore not affected by the different direction sensitivity.



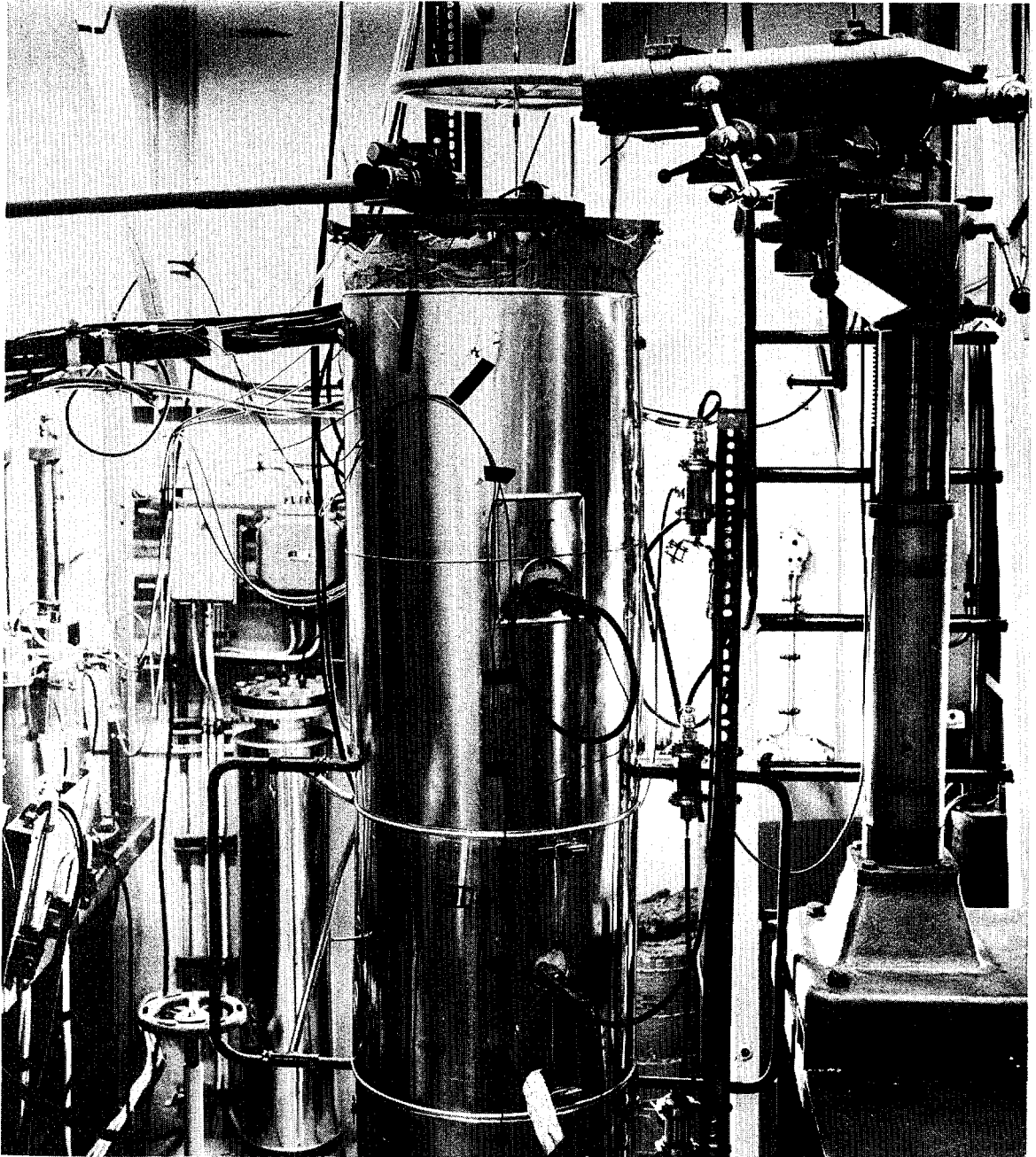


Fig. 3. Outlet of the air rig and traverse device.

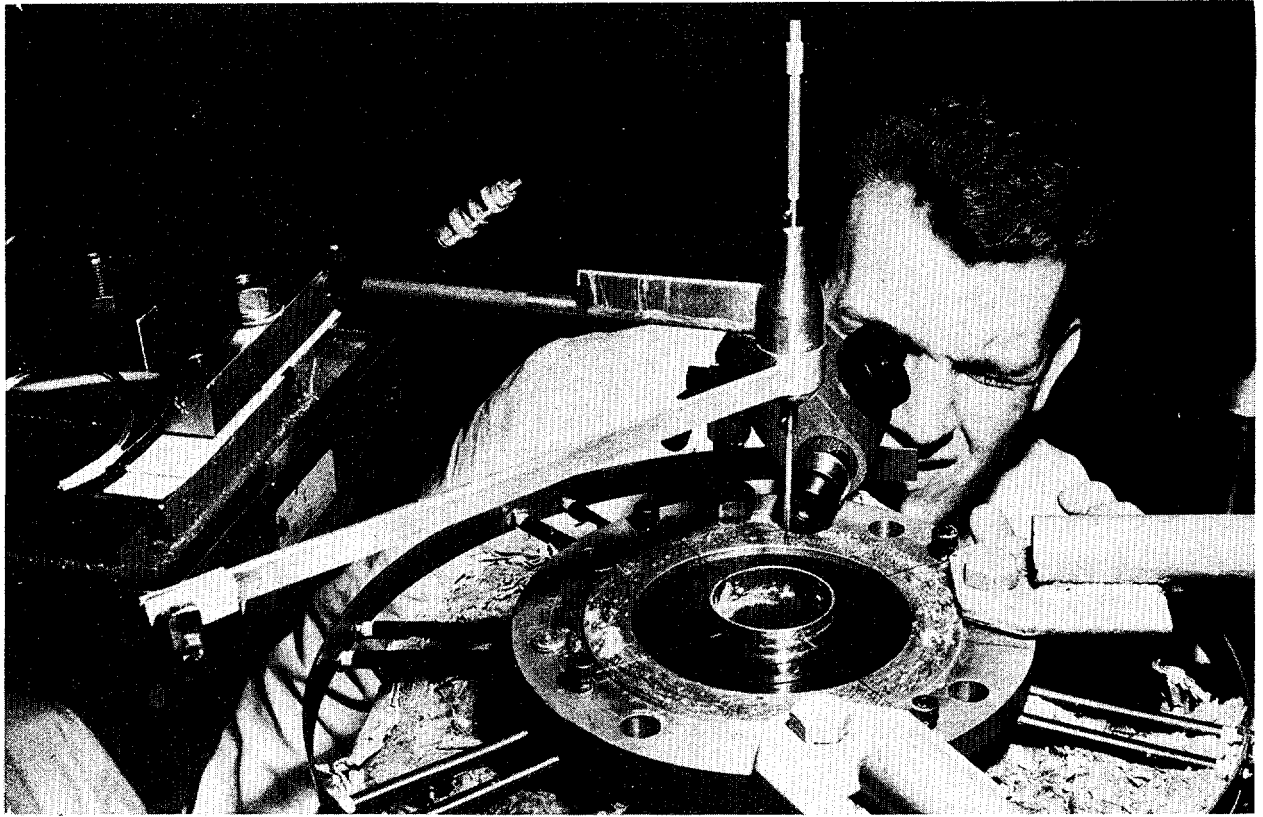


Fig. 4a. Original probe support.

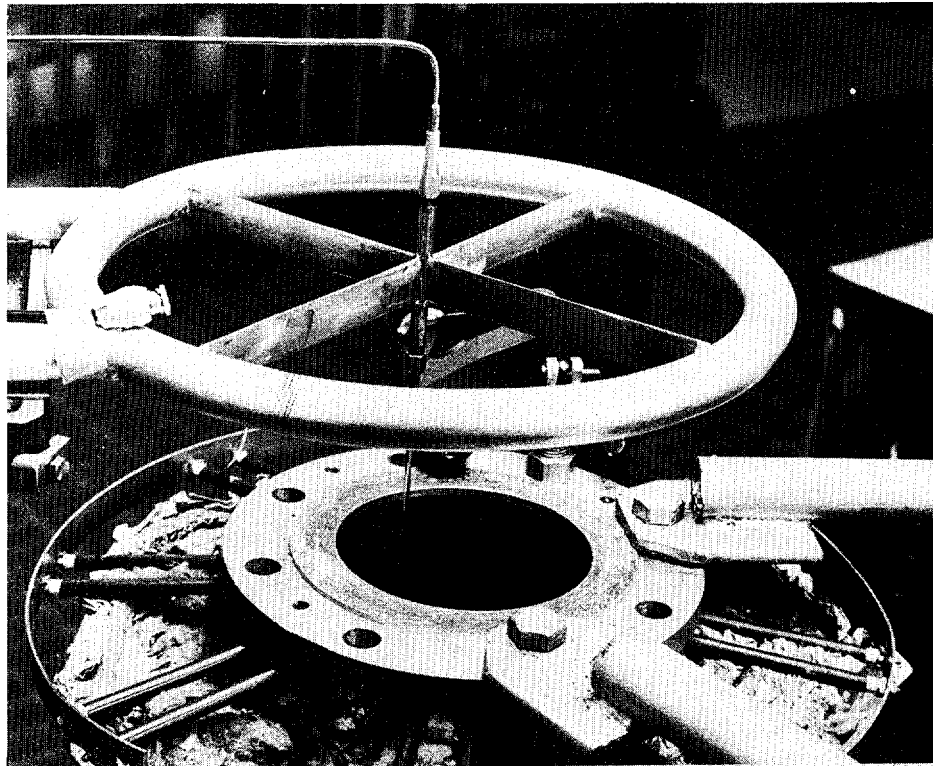
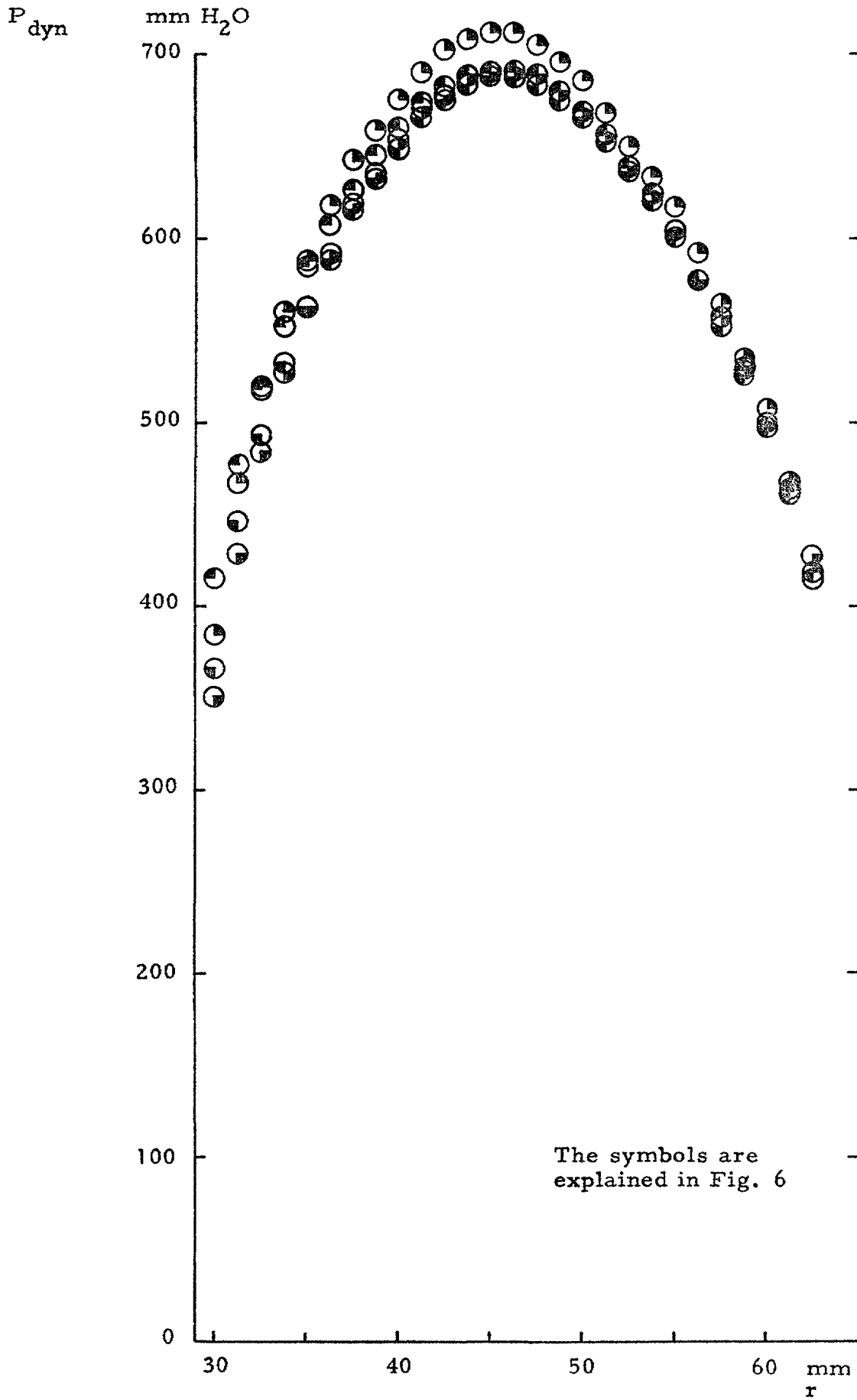


Fig. 4b. Modified probe support.

Test rod: A
smooth

Dynamic pressure distribution at outlet

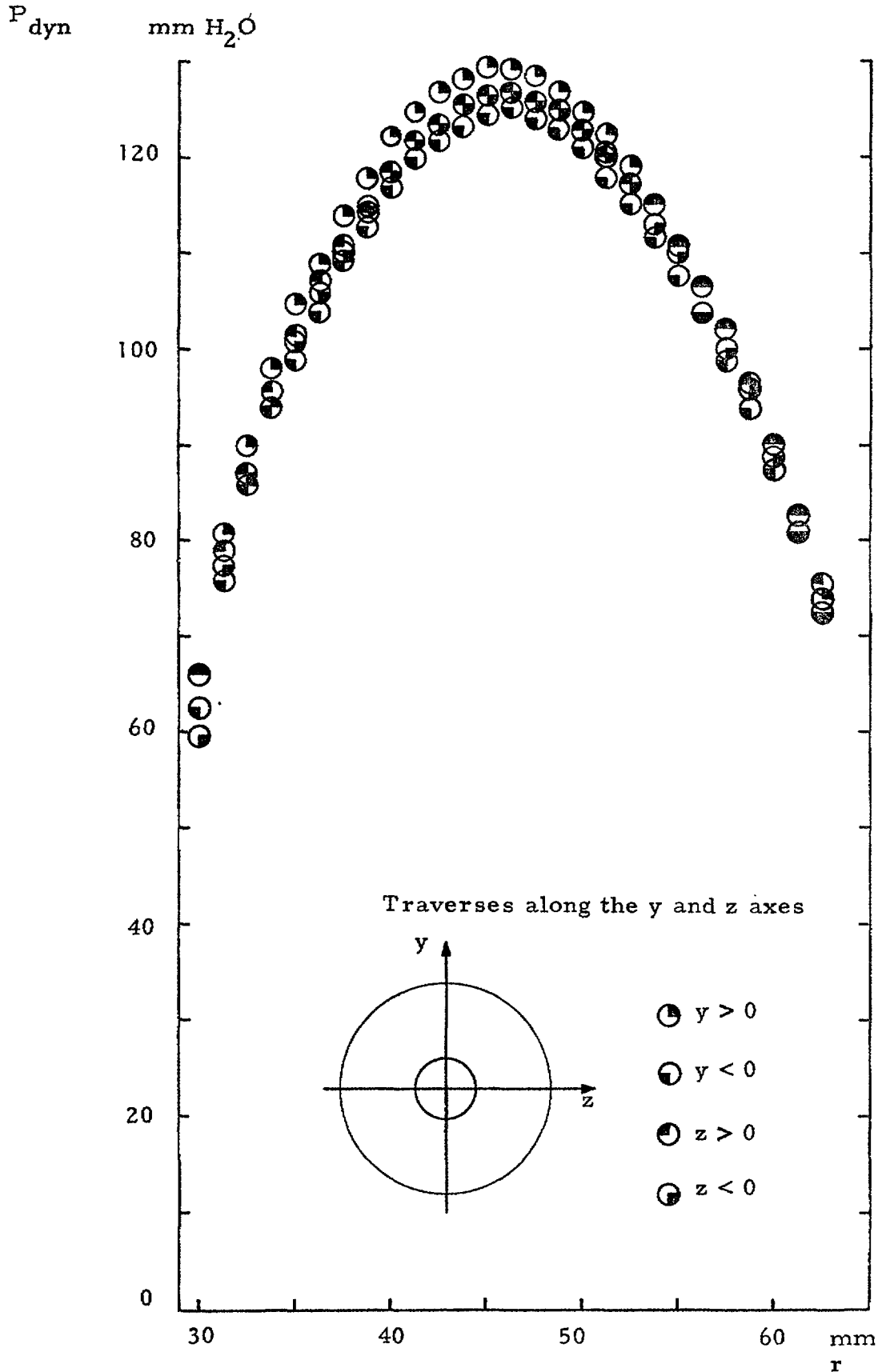
Fig. 5



Test rod: A
smooth

Dynamic pressure distribution at outlet

Fig. 6



$\ln(V^2 - V_0^2)$

4.5

Collis' law:
 $(V^2 - V_0^2) = A \cdot \bar{u}^c$

4.4

4.3

4.2

4.1

4.0

3.9

3.8

3.6 3.7 3.8 3.9 4.0 4.1 4.2 4.3 4.4 4.5 4.6 4.7

$\ln \bar{u}$

Test run	Normal wire Symbol	c	Slanting wire Symbol	c
A5053	▽	0.400	▽	0.442
A5058	○	0.455	●	0.480
A5063	◇	0.430	◇	0.430
A5068	△	0.434	▲	0.440

Determination of the exponent c in
 Collis' law
 Experiments in annular channel with
 smooth rod.

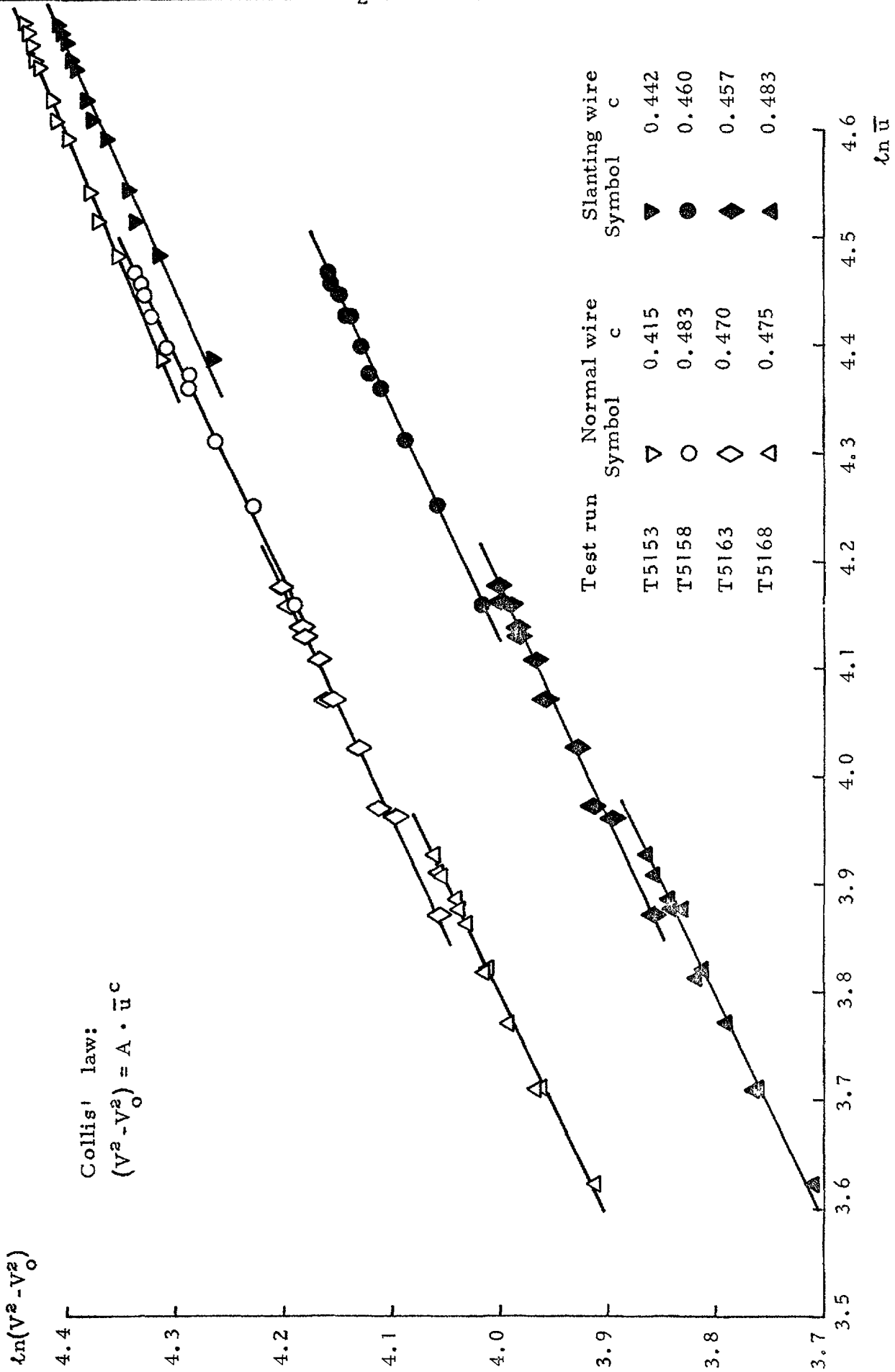
Fig. 7

Determination of the exponent c in

Collis' law

Experiments in annular channel with rough rod T_2

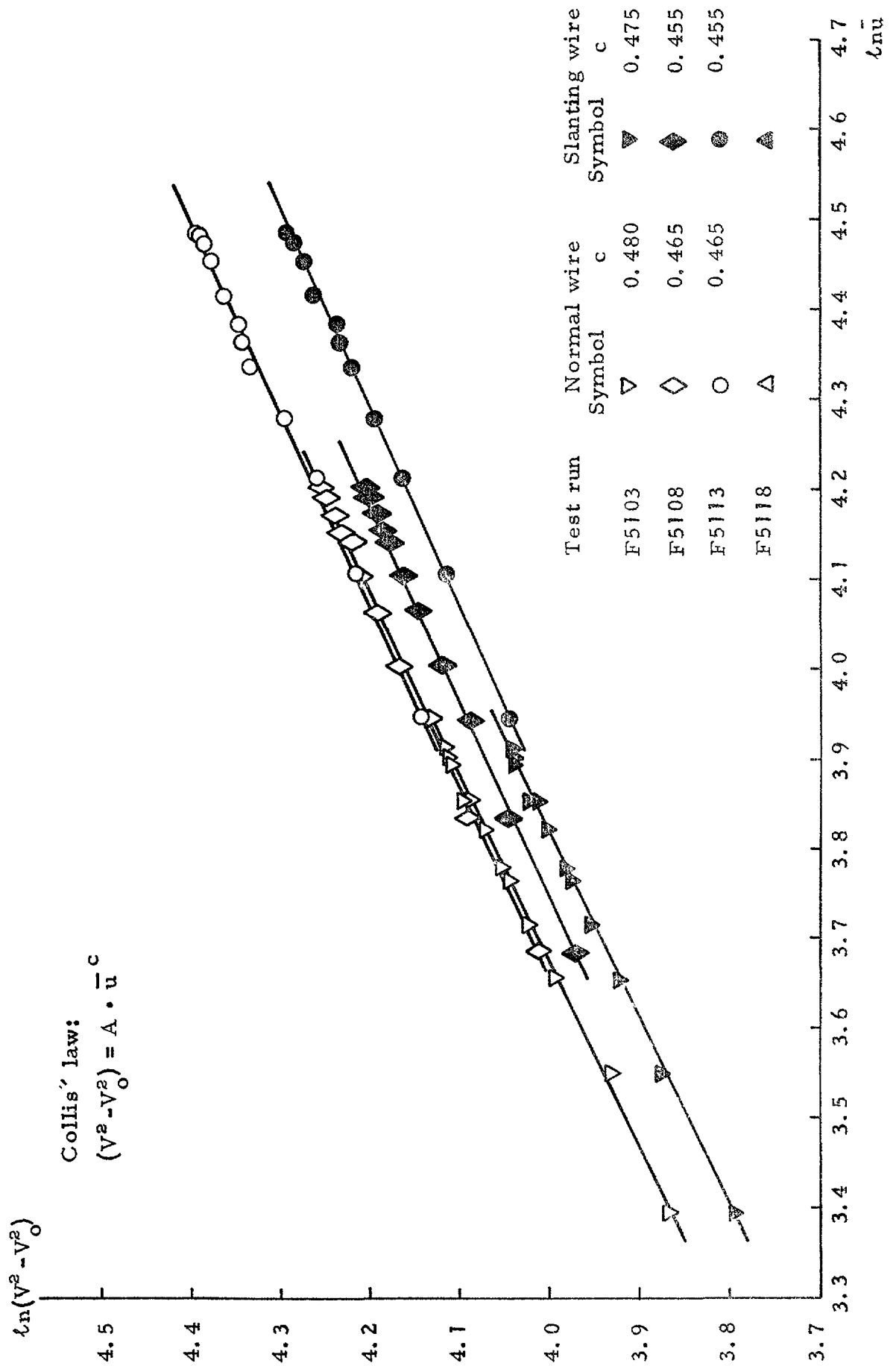
Fig. 8



Determination of the exponent c in Collis' law.

Experiments in annular channel with rough rod F.

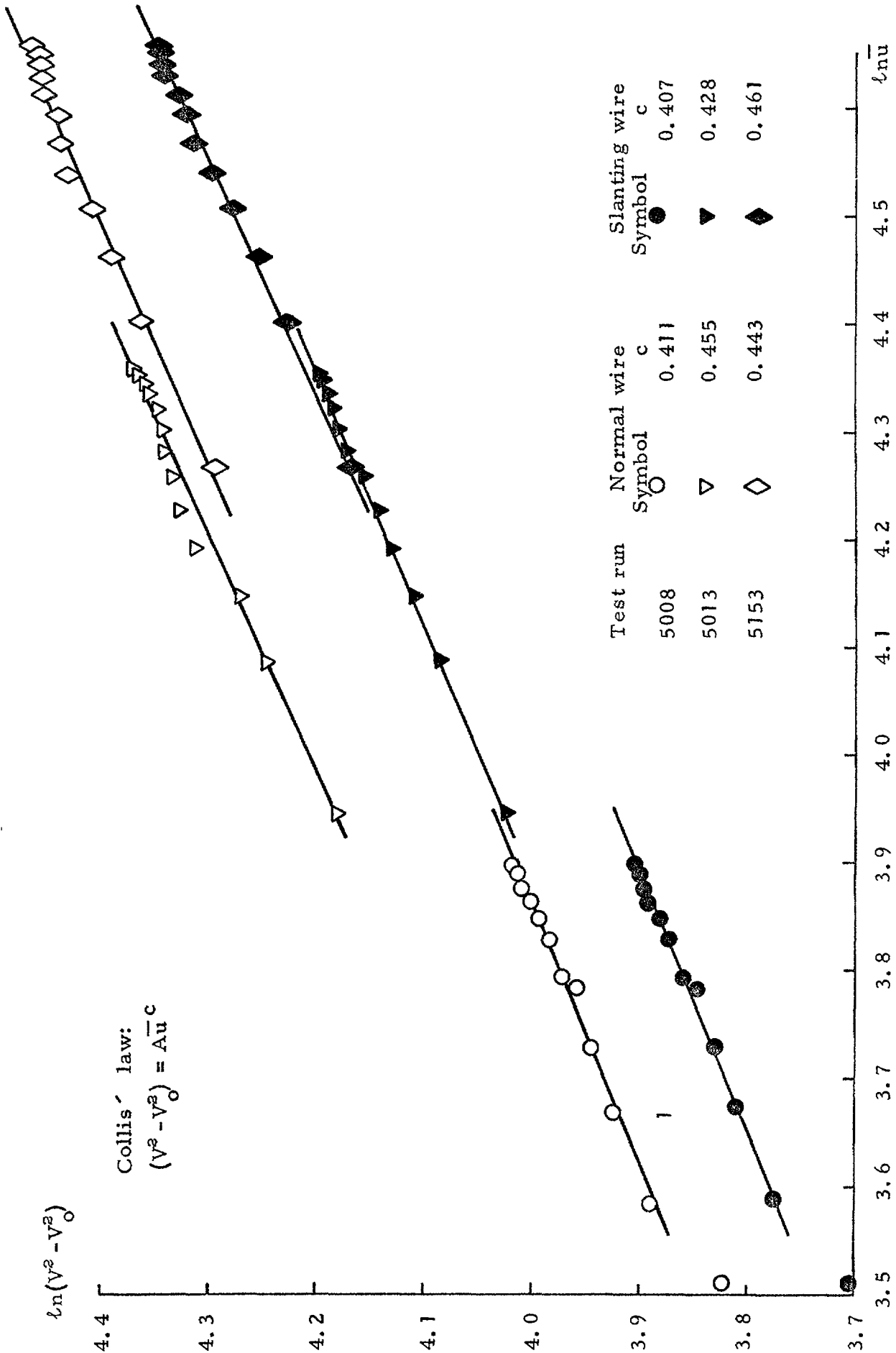
Fig. 9



Determination of the exponent c in Collis' law.

Experiments in smooth circular channel.

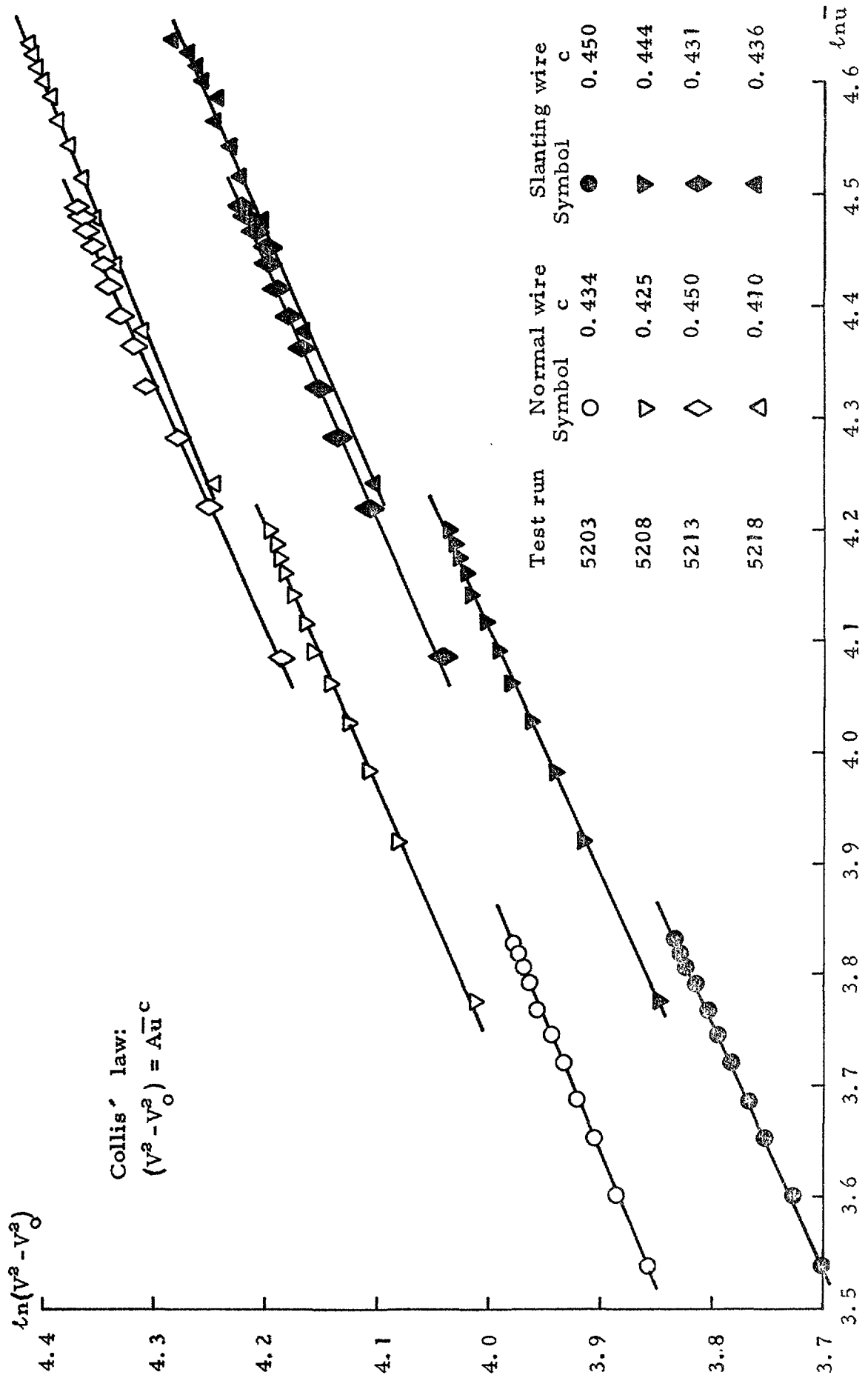
Fig. 10



Determination of the exponent c in Collis' law.

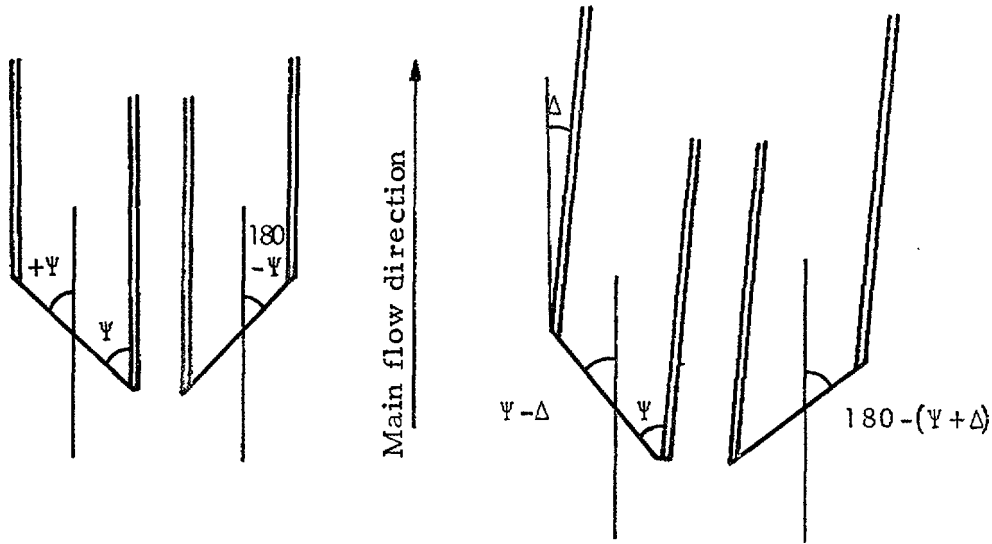
Experiments in smooth circular channel.

Fig. 11



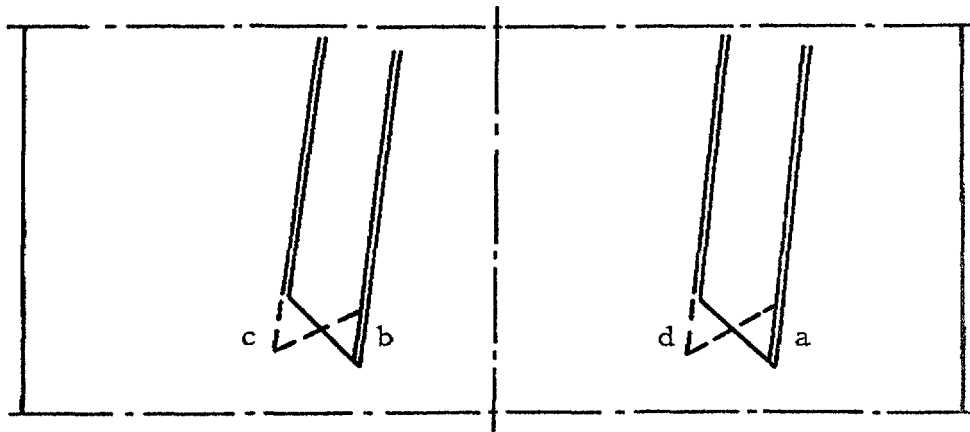
Effect of an inclined probe support on the yaw angle.

Fig. 12



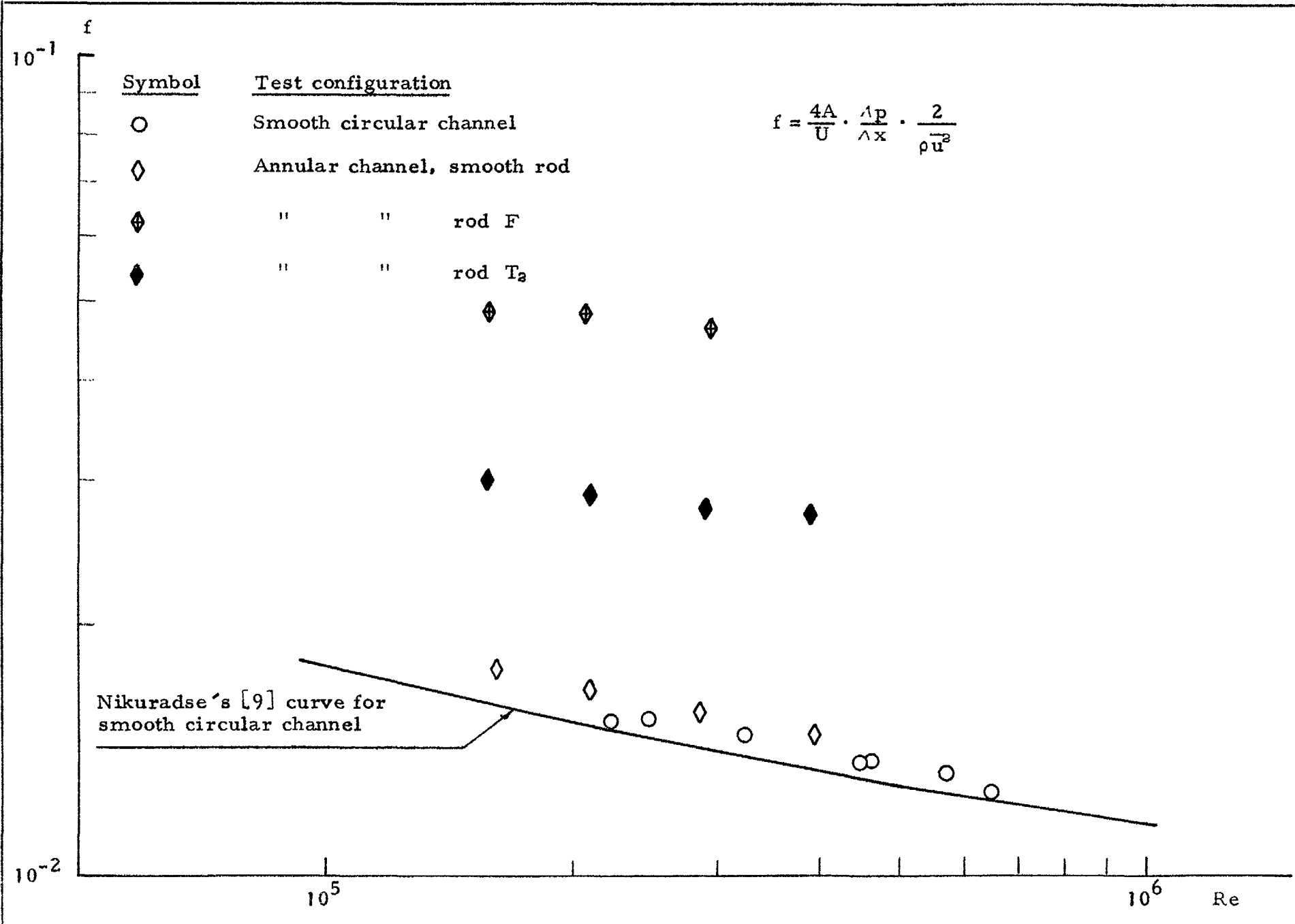
Ideal case. Probe axis parallel to main flow direction

Actual case. Probe axis inclined to main flow direction



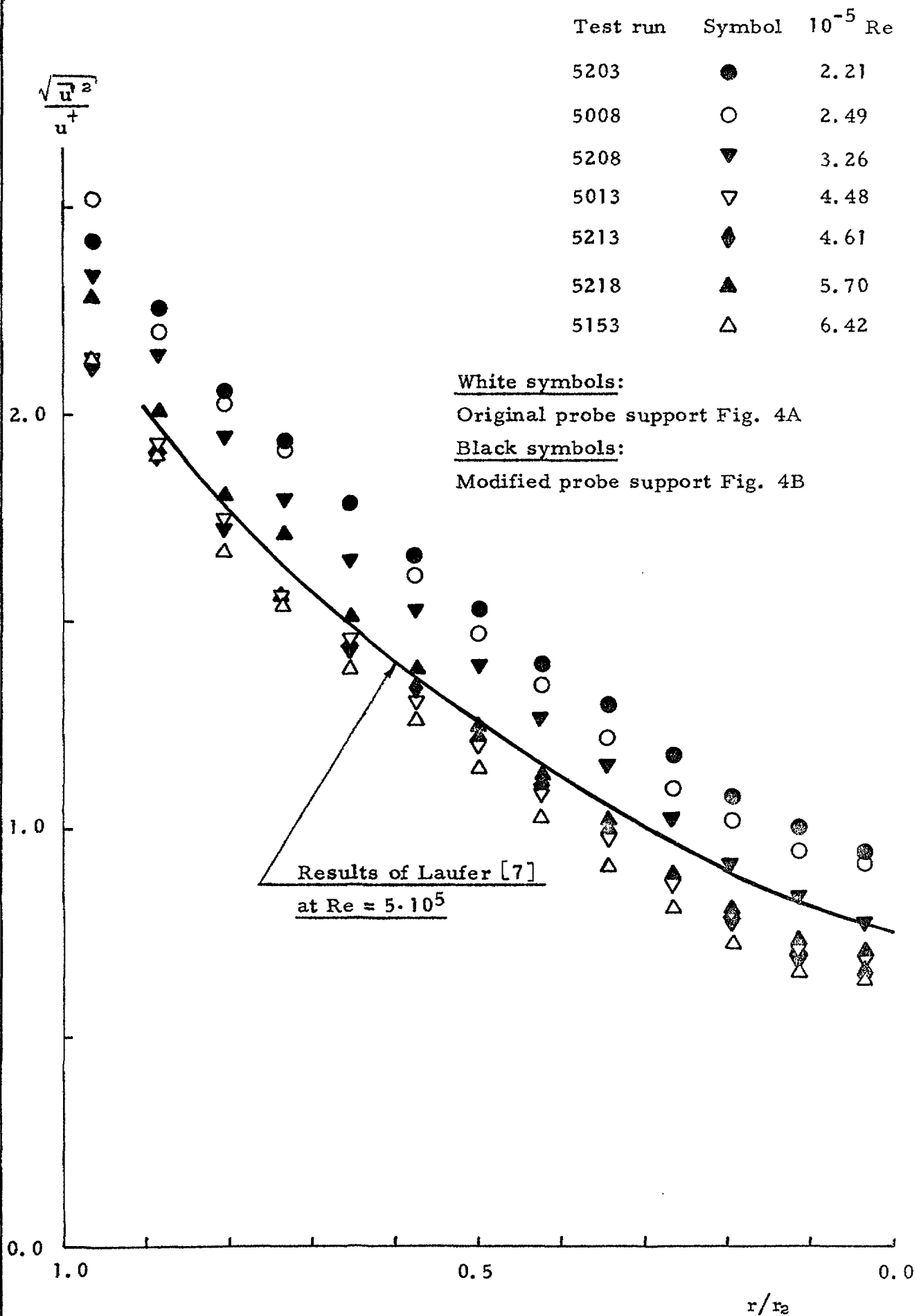
Traverse across a circularly symmetric channel

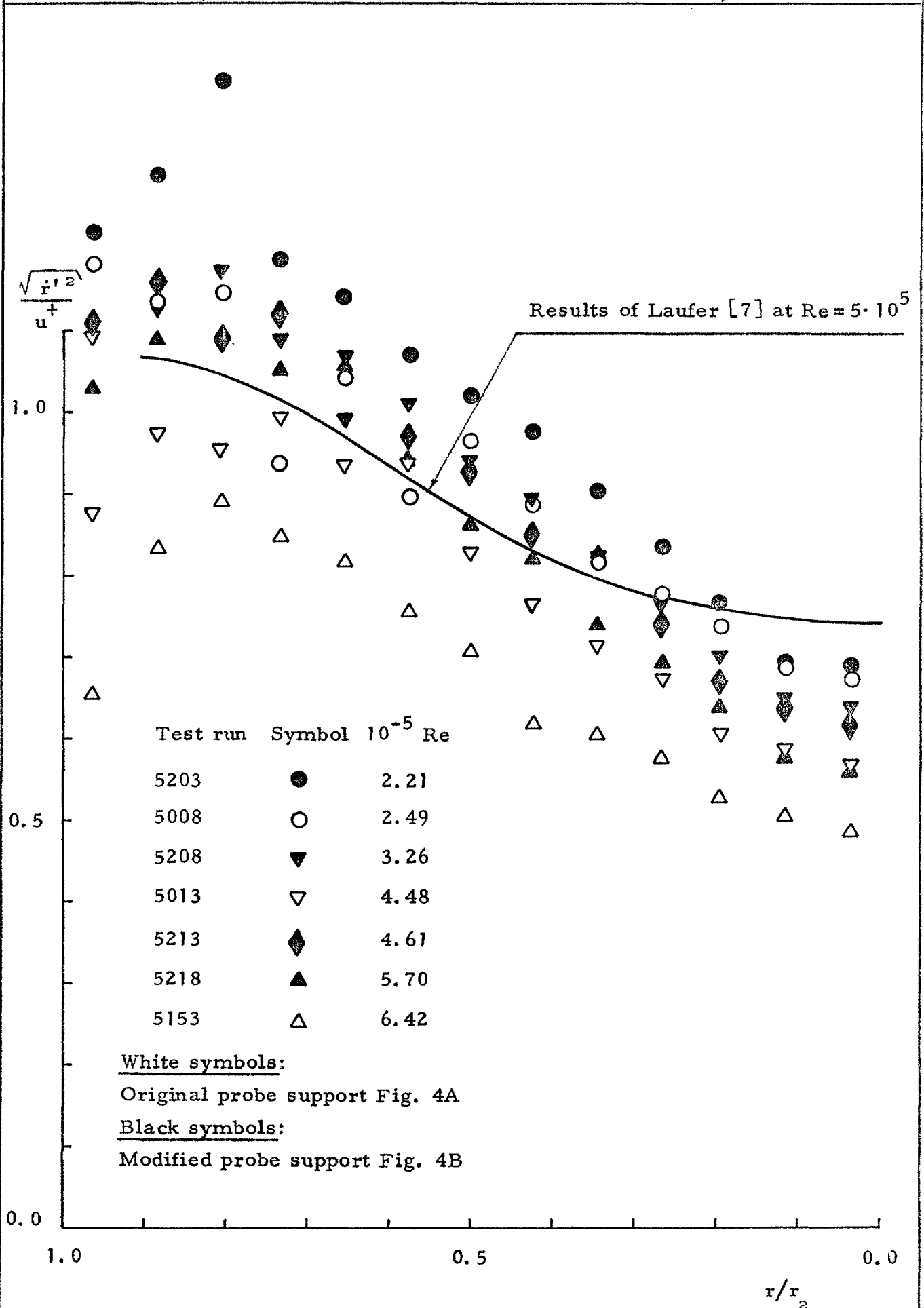
The yaw angles to the flow will be the same but with opposite signs for cases a and b and for cases c and d. If mean values are taken of measurements for a and c, b and d, they will be approximately valid for yaw angles Ψ and $180 - \Psi$.



Measured total friction factors (defined for entire channel) vs. total Reynolds number.

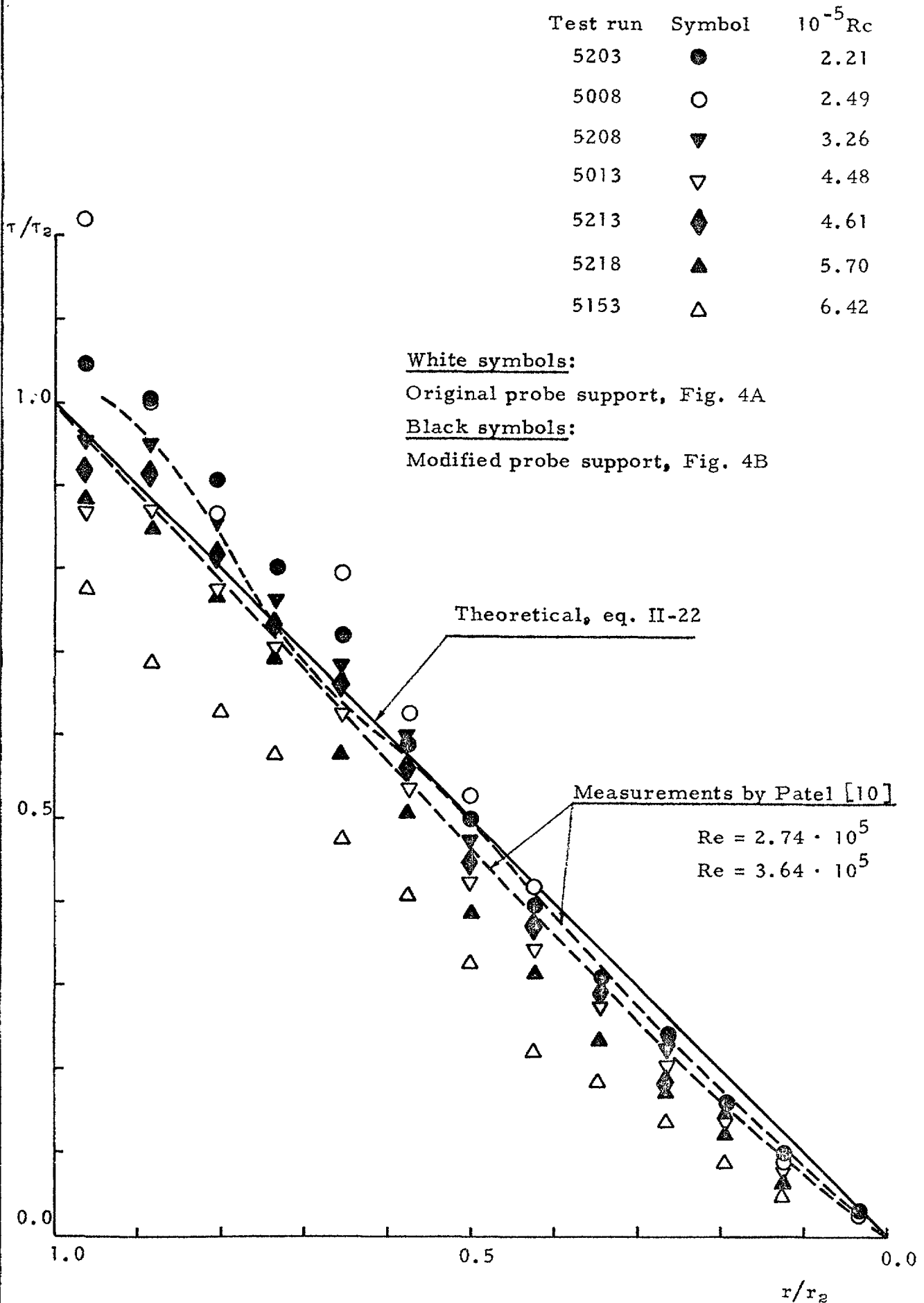
Fig. 13





Shear stress distributions measured
in smooth circular channel

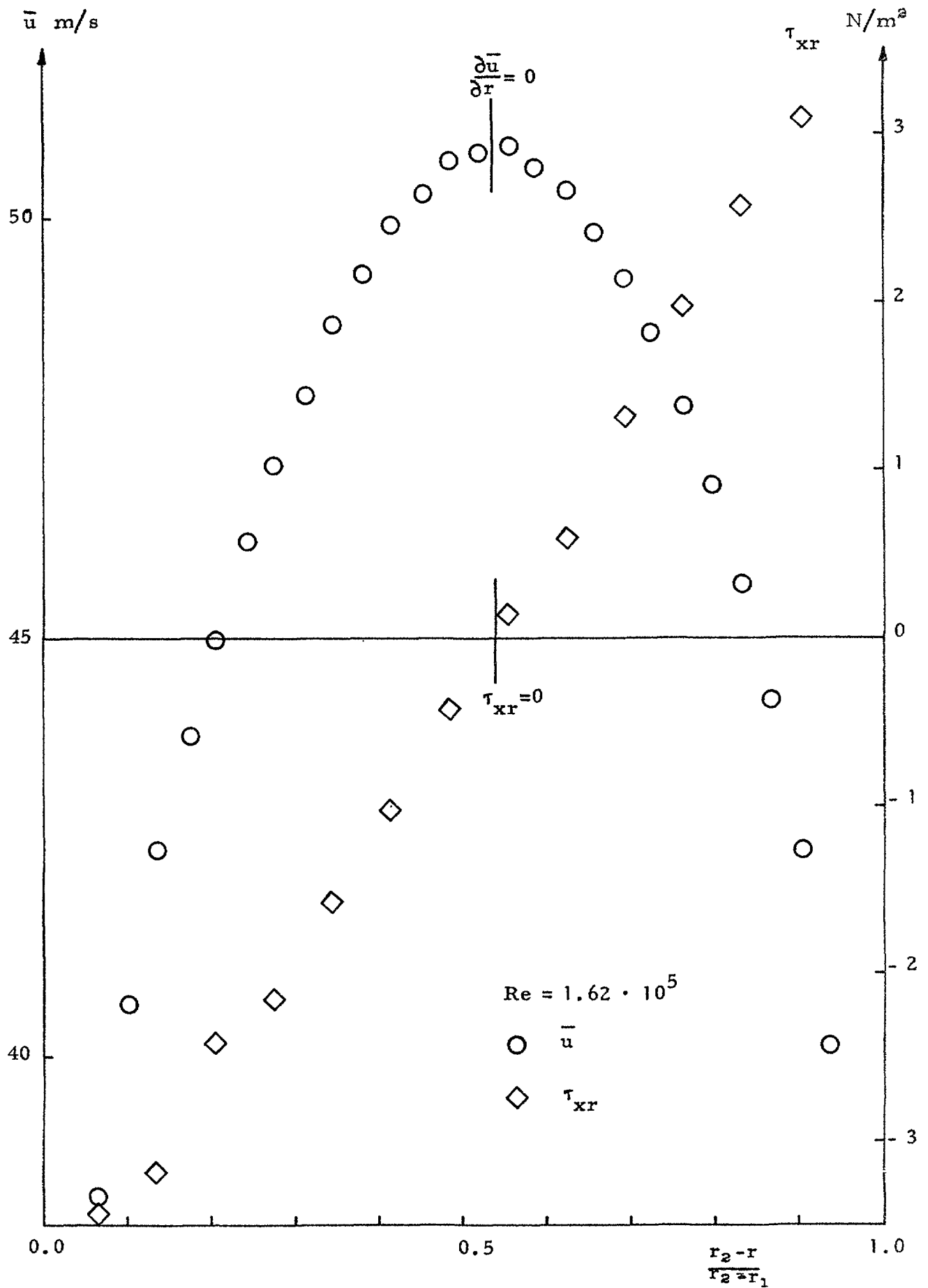
Fig. 16



Test rod: A
smooth

Velocity and shear stress distribution
in smooth annulus

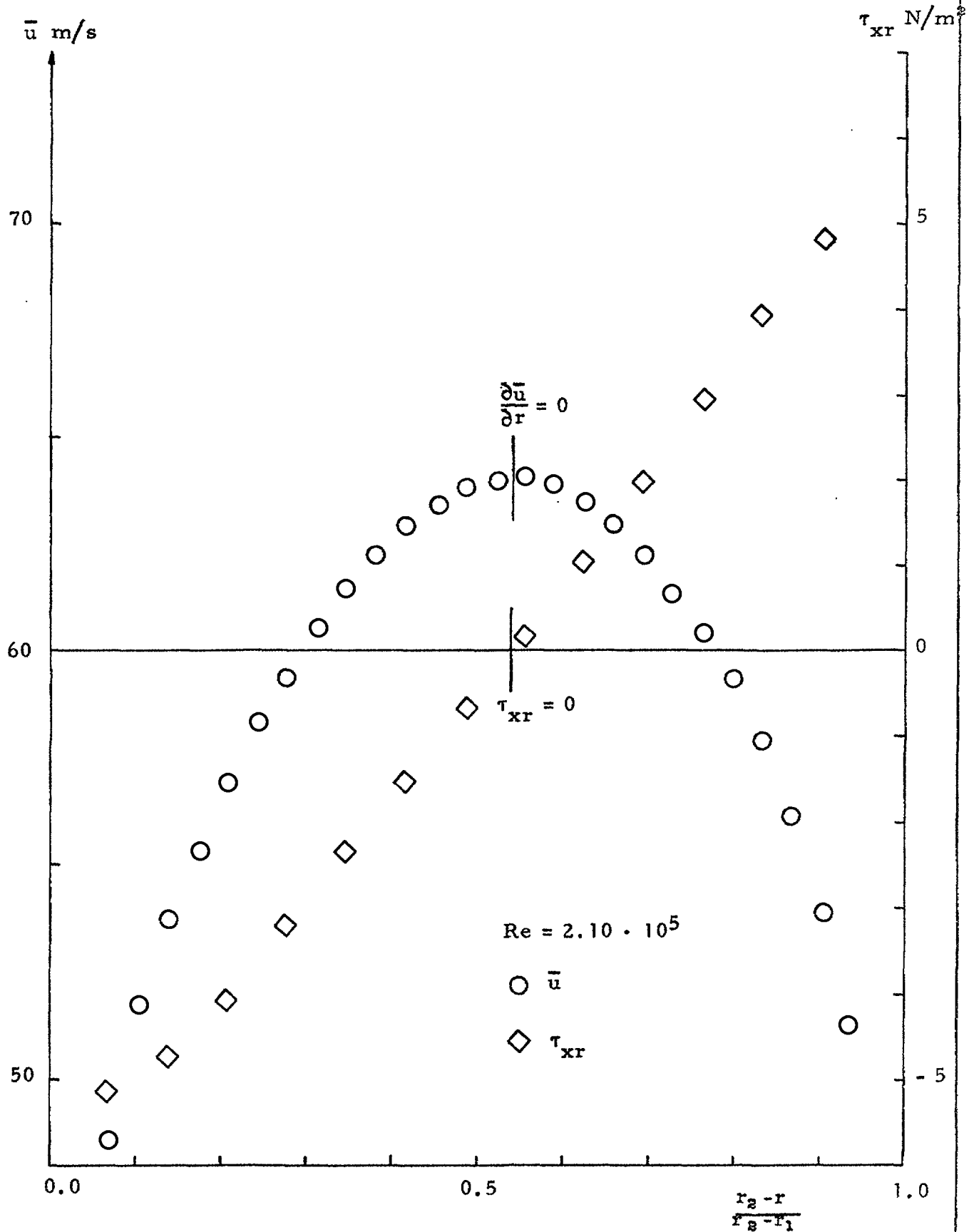
Fig. 17



Test rod: A
smooth

Velocity and shear stress distribu-
tion in smooth annulus

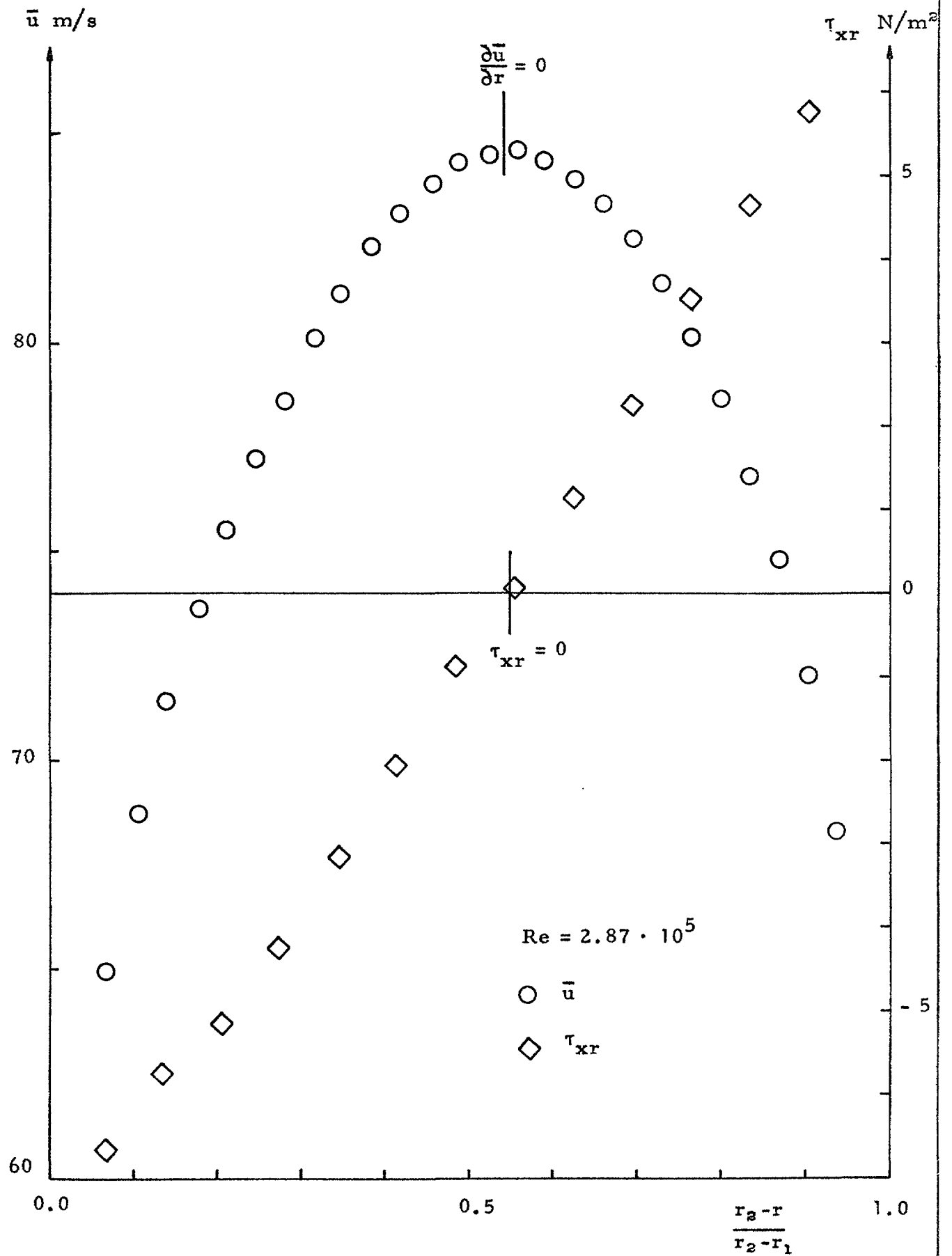
Fig. 18



Test rod: A
smooth

Velocity and shear stress distribu-
tion in smooth annulus

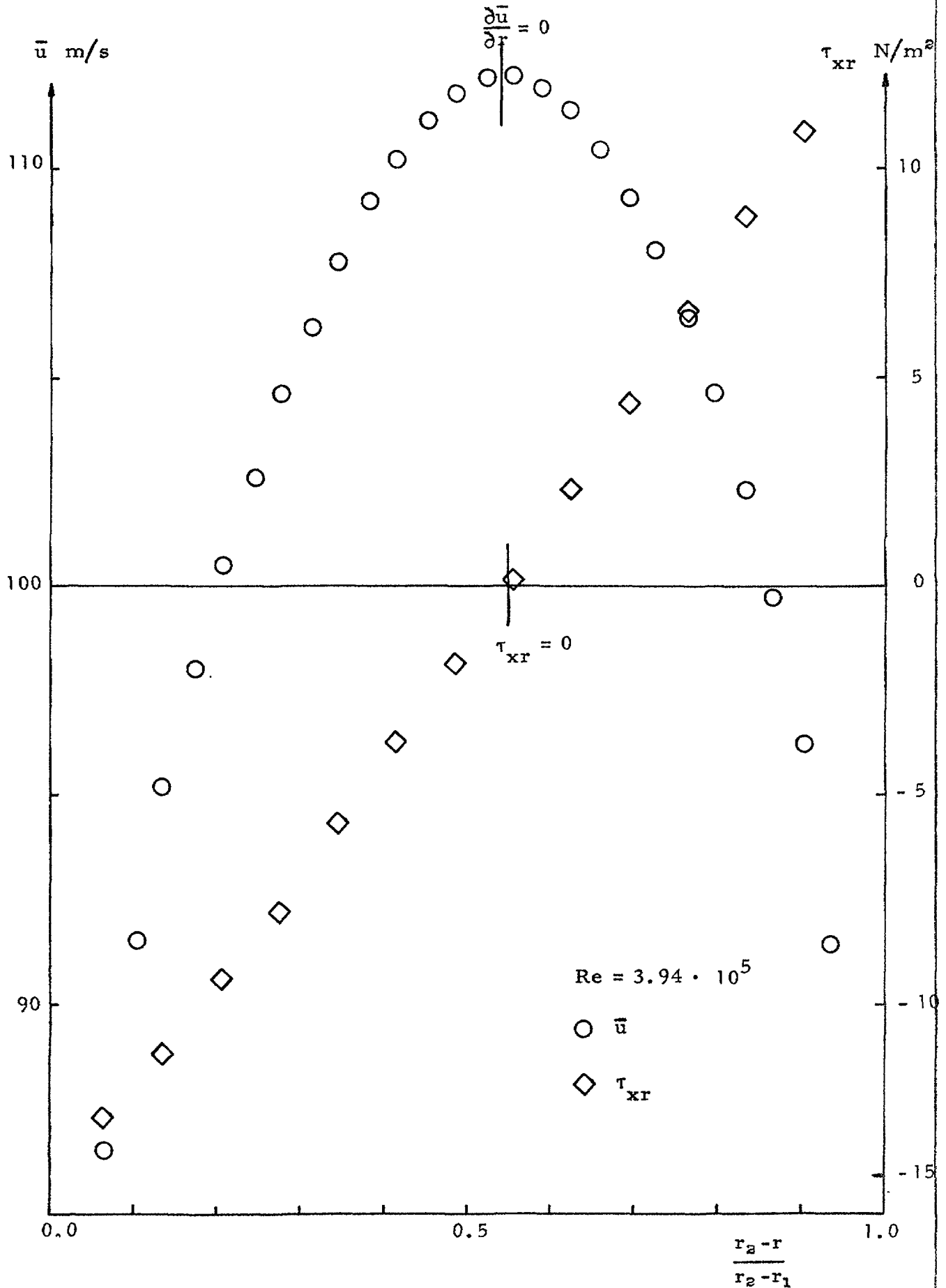
Fig. 19



Test rod: A
smooth

Velocity and shear stress distribu-
tions in smooth annulus

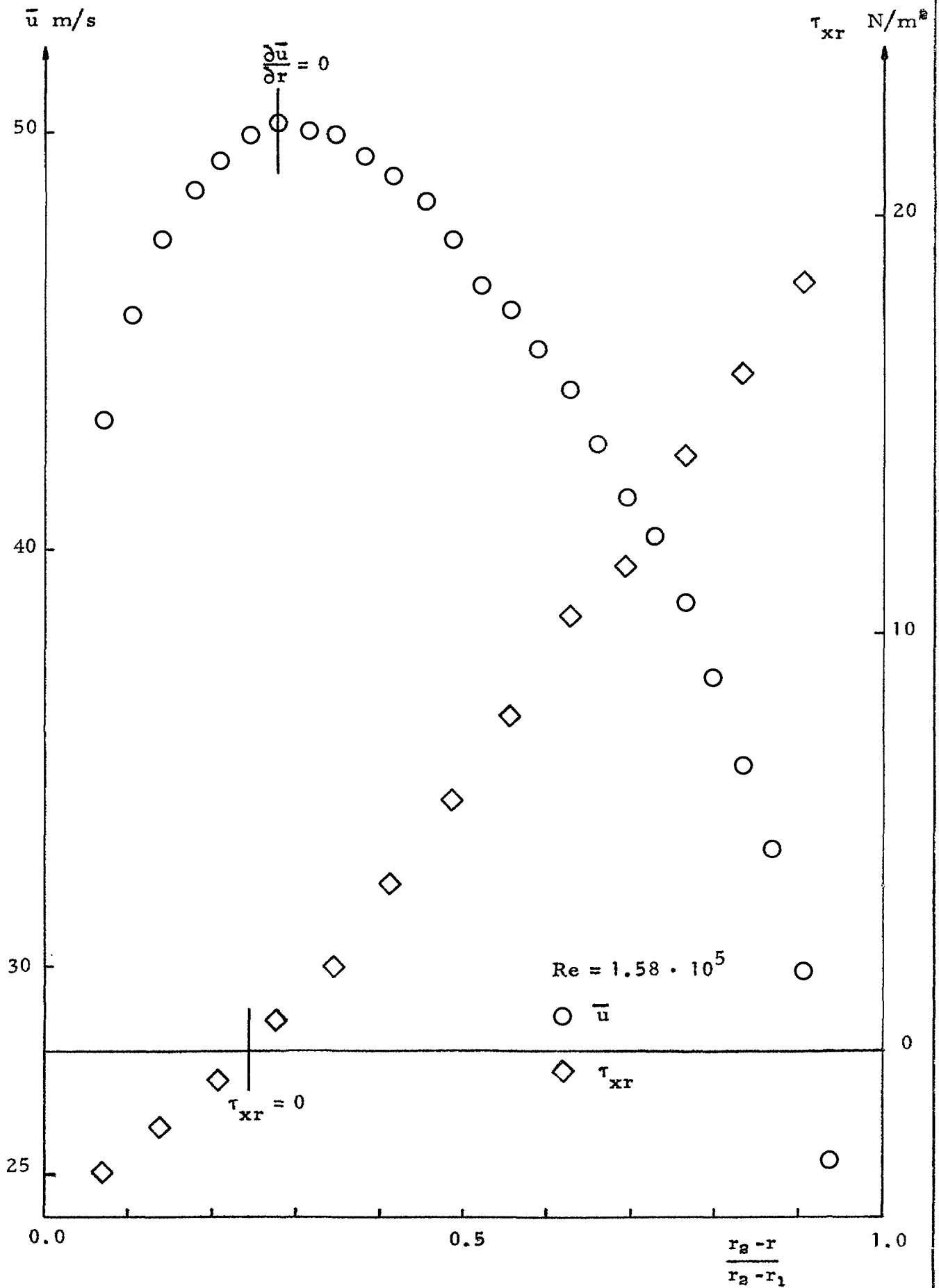
Fig. 20



Test rod: F
 rect. fins.
 $h=0.93$ mm
 $s/h=8.6$

Velocity and shear stress distributions in an
 annulus with smooth outer surface and rough
 inner surface

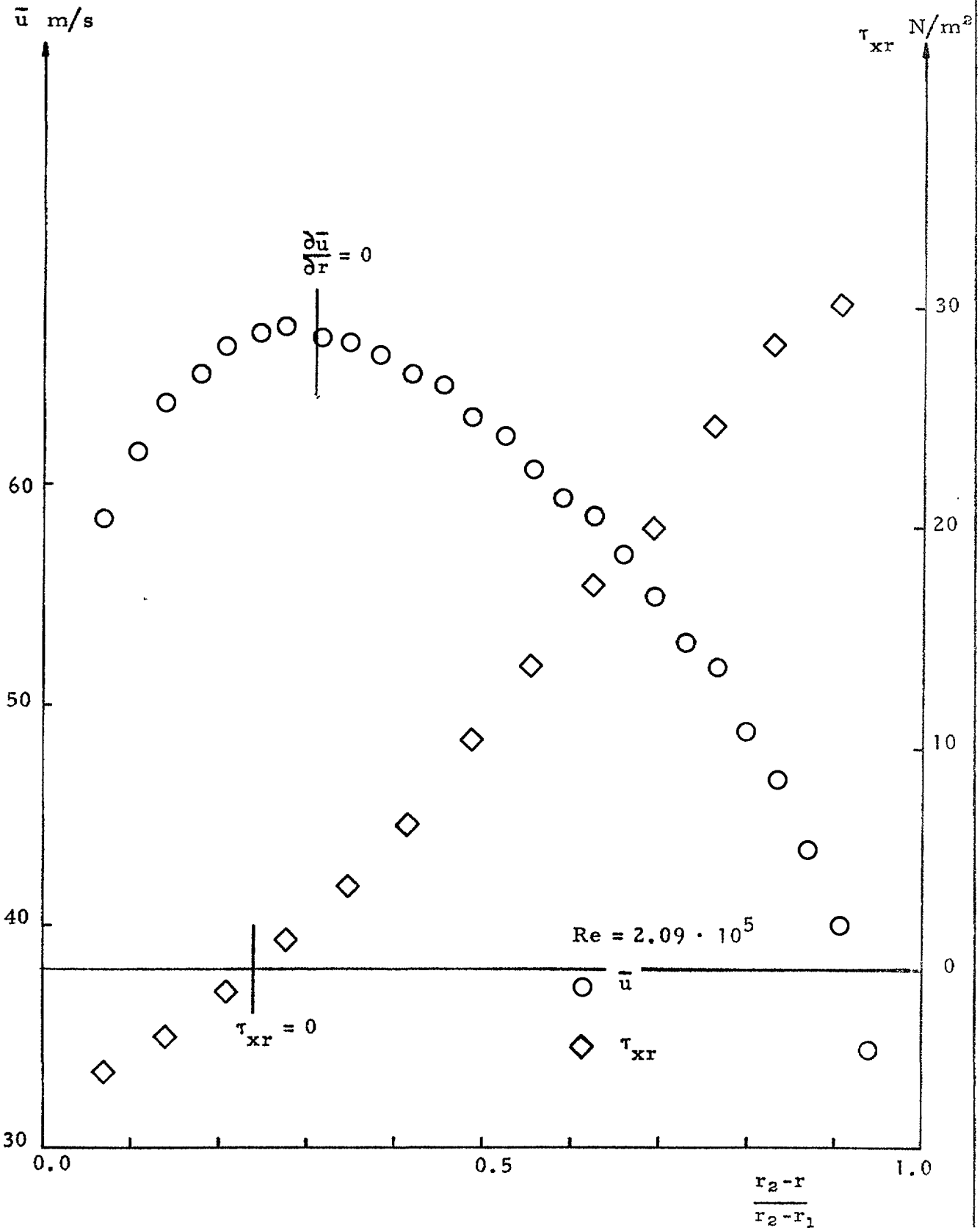
Fig. 21



Test rod: F
 rect. fins.
 $h=0.93$ mm
 $s/h=8.6$

Velocity and shear stress distributions in an
 annulus with smooth outer surface and rough
 inner surface

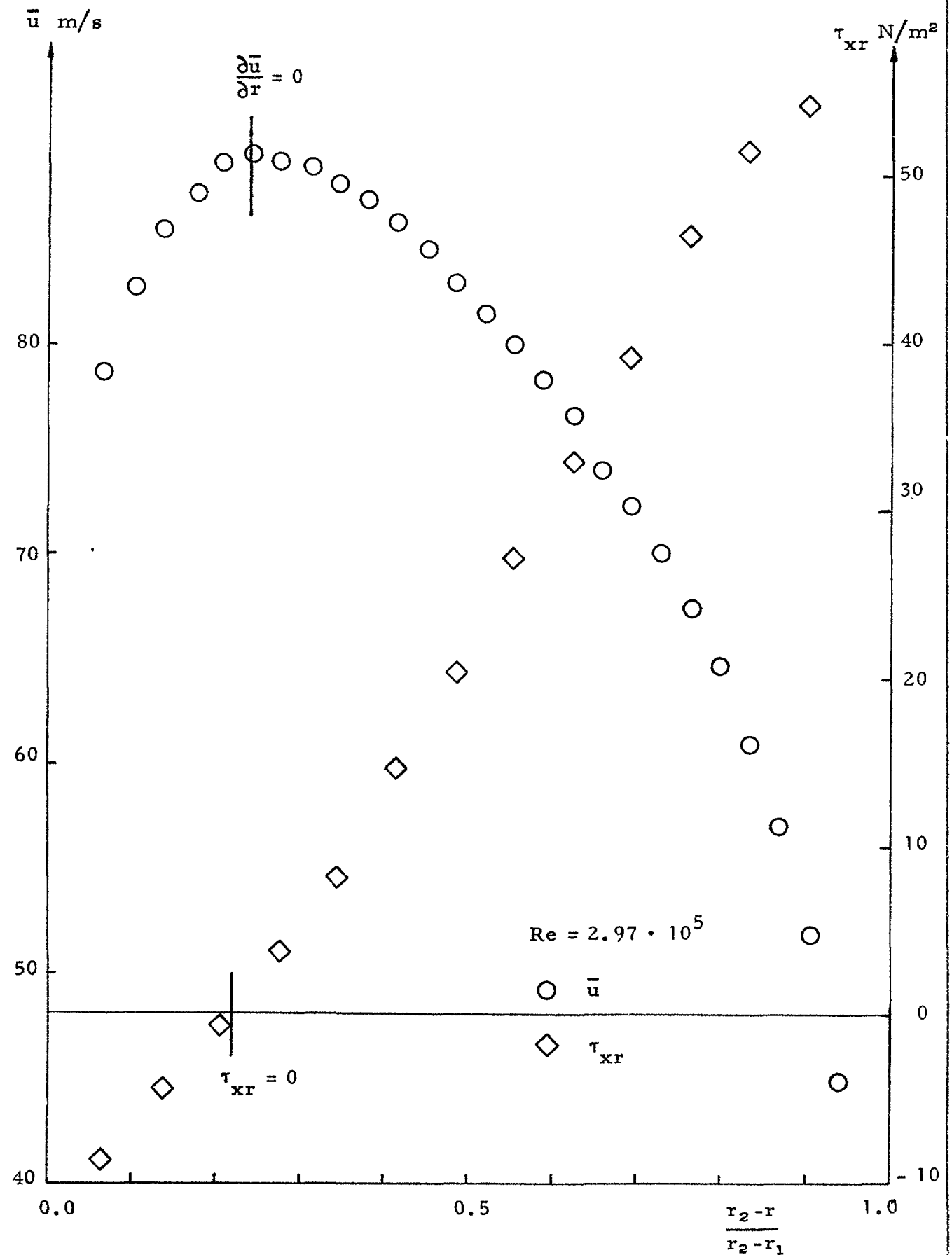
Fig. 22



Test rod: F
rect. fins.
 $h=0.93$ mm
 $s/h=8.6$

Velocity and shear stress distributions in
an annulus with smooth outer surface and
rough inner surface

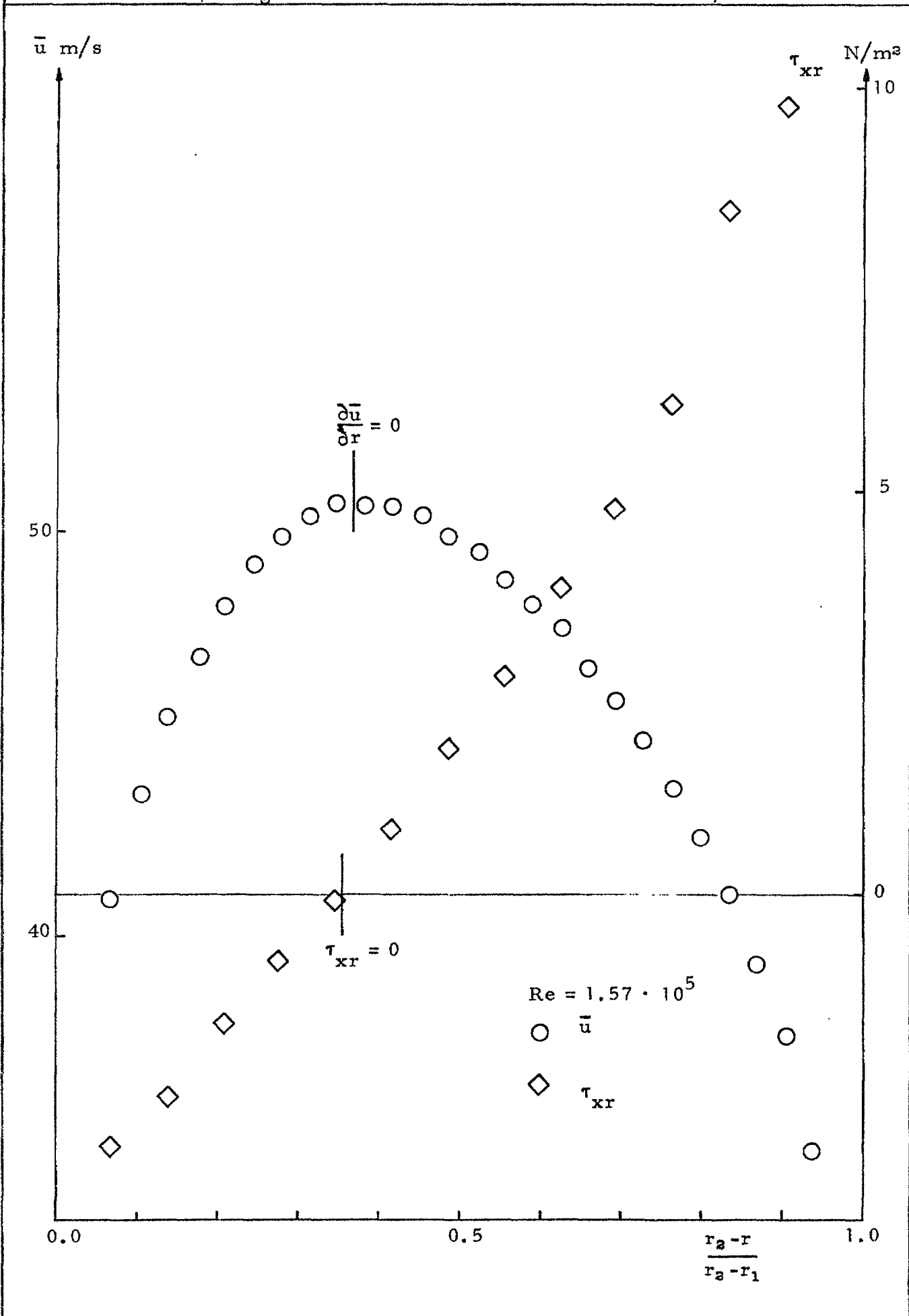
Fig. 23



Test rod: T
sawtooth fins
 $h=0.74$ mm
 $s/h=15.0$

Velocity and shear stress distribution in
an annulus with smooth outer surface and
rough inner surface

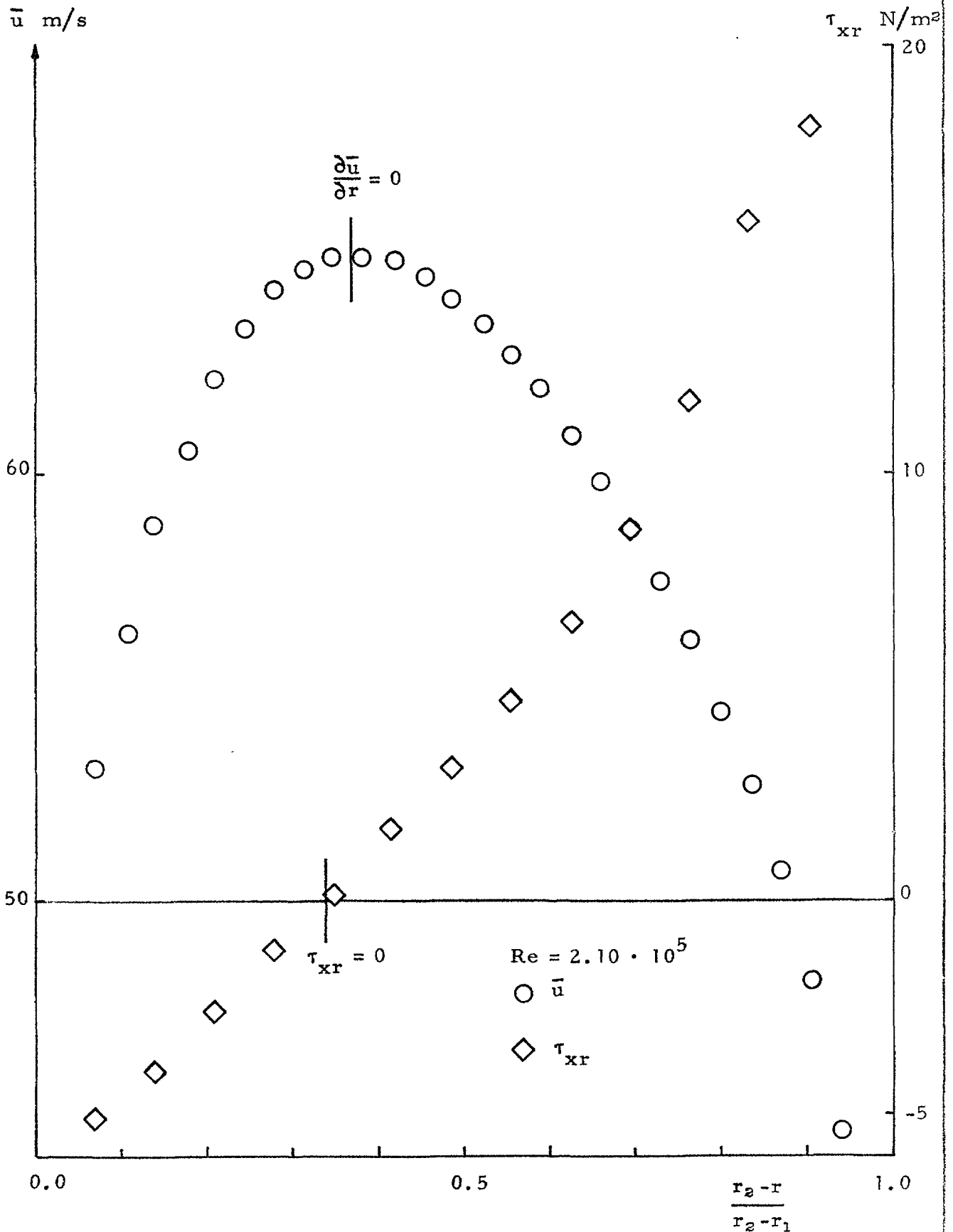
Fig. 24



Test rod: T
sawtooth fins
 $h=0.74$ mm
 $s/h=15.0$

Velocity and shear stress distributions in
an annulus with smooth outer surface and
rough inner surface

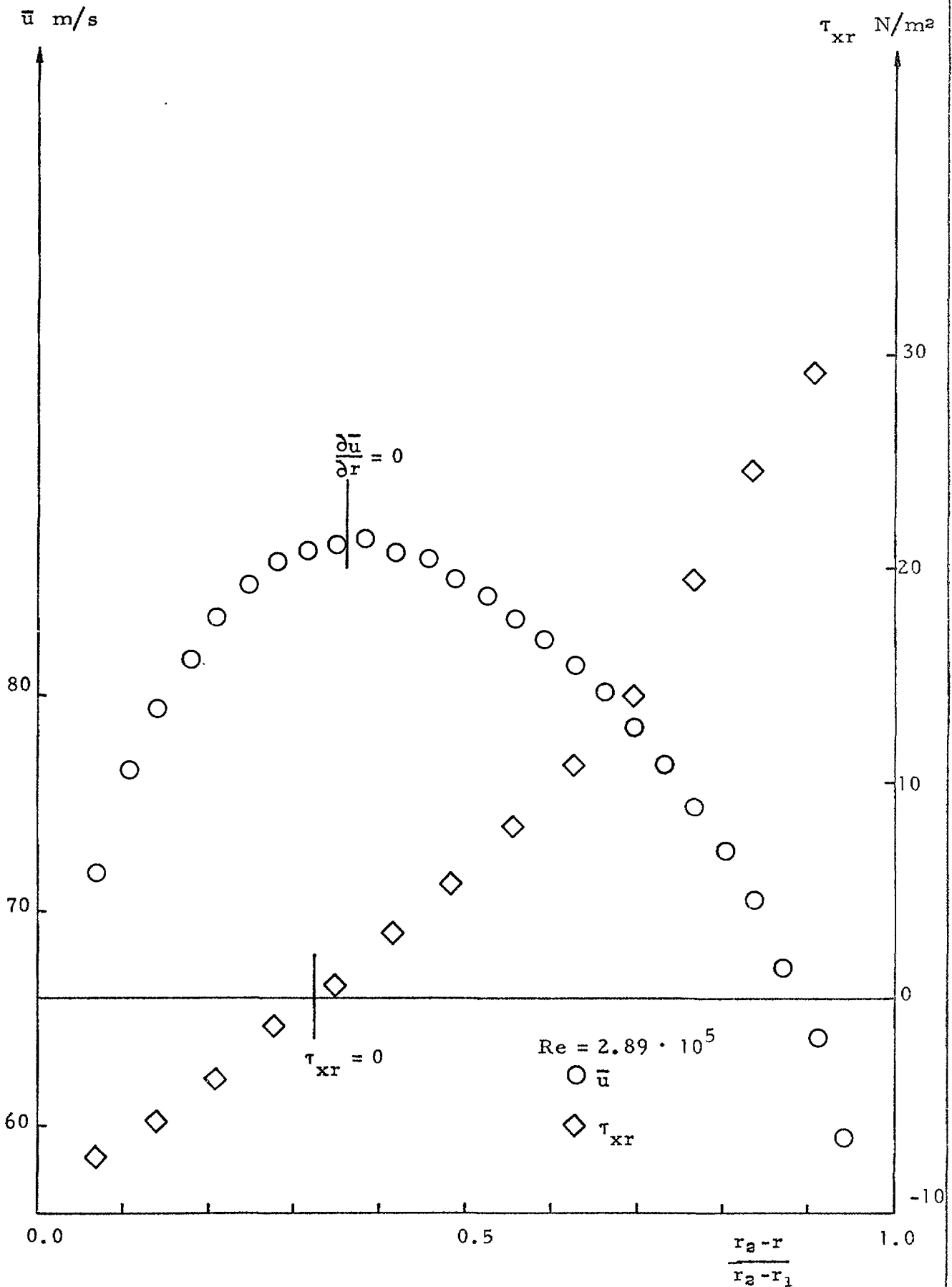
Fig. 25



Test rod: T
sawtooth fins
 $h=0.74$ mm
 $s/h=15.0$

Velocity and shear stress distributions in
an annulus with smooth outer surface and
rough inner surface

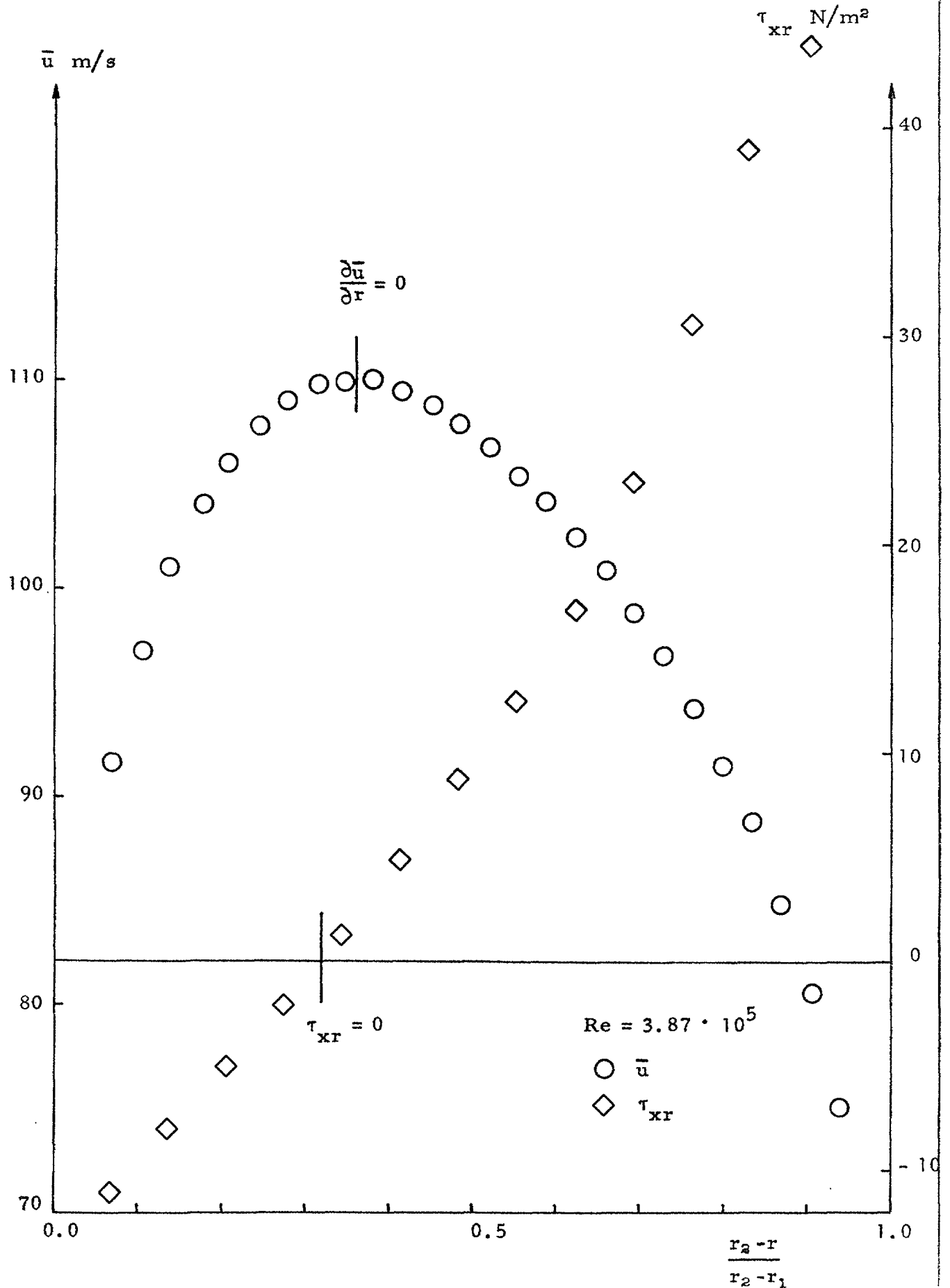
Fig. 26



Test rod: T
 sawtooth fins
 $h=0.74$ mm
 $s/h=15.0$

Velocity and shear stress distributions in
 an annulus with smooth outer surface and
 rough inner surface

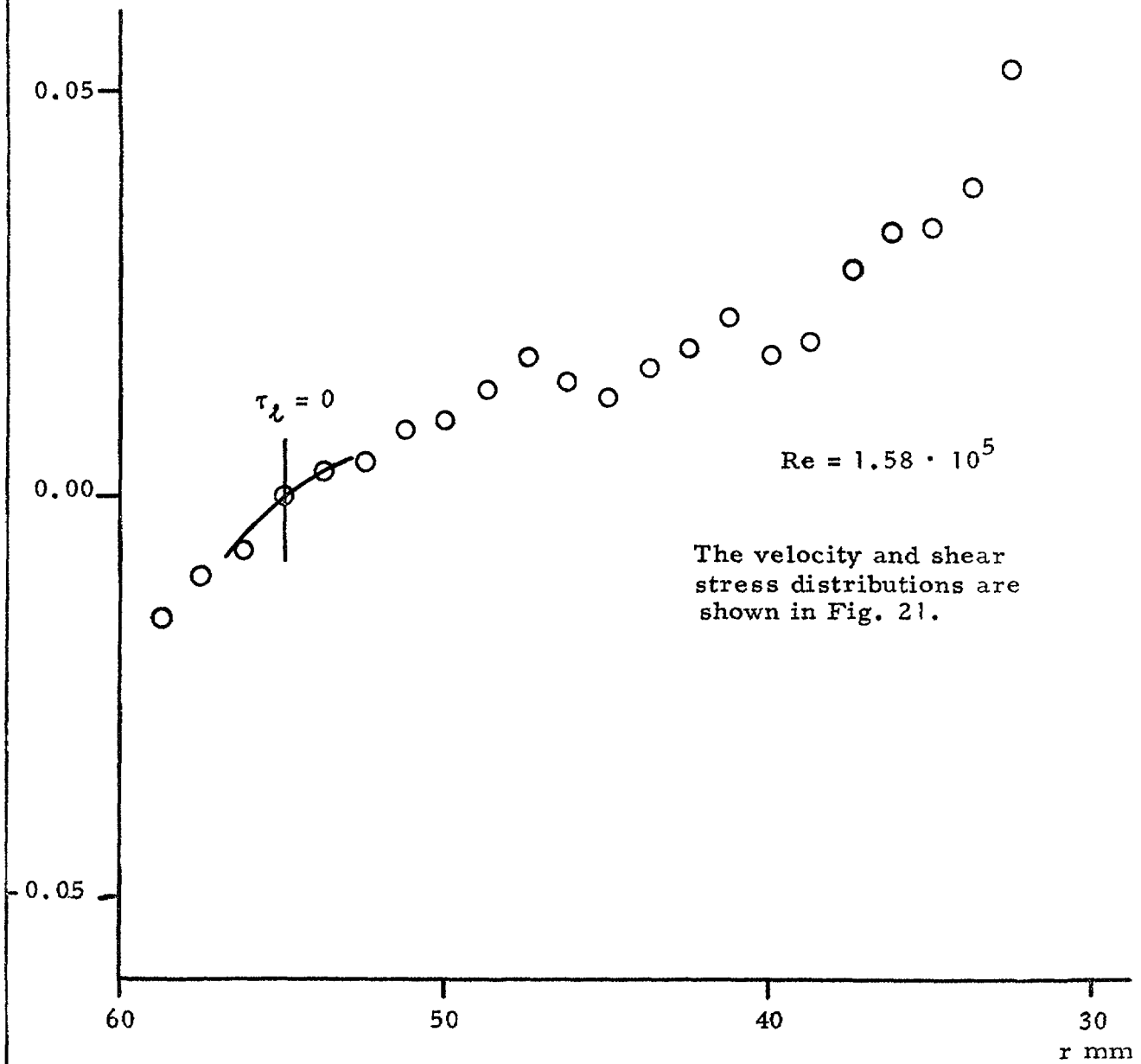
Fig. 27



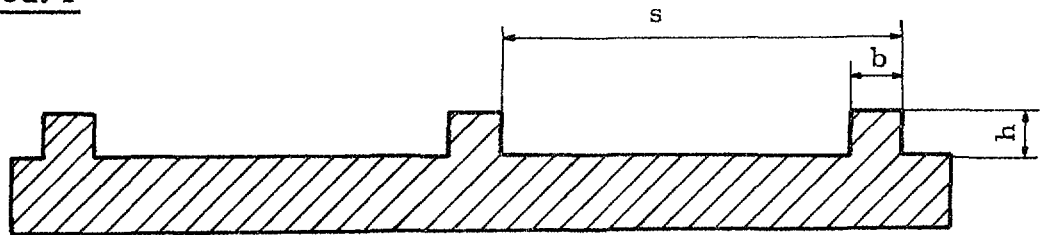
Test rod: F

Distribution of the laminar shear stress
calculated from the velocity distribution
by eq. II-6

Fig. 28

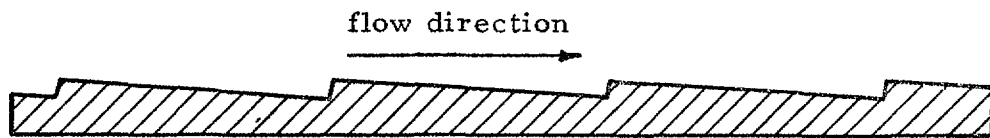


Test rod: F



Scale: 0 2 4 6 8 10 mm

Test rod: T



Scale: 0 5 10 15 20 mm

Fin-dimensions

Test rod	h mm	σ_h mm	s/h	$\sigma_{s/h}$	s/b	$\sigma_{s/b}$
F	0.931	0.042	8.62	0.35	7.97	0.22
T	0.739	0.056	14.97	0.99	-	-

Root diameter of fins: 58.0 mm

LIST OF PUBLISHED AE-REPORTS

- 1-170. (See the back cover earlier reports.)
171. Measurements on background and fall-out radioactivity in samples from the Baltic bay of Tvären, 1957-1963. By P. O. Agnedal. 1965. 48 p. Sw. cr. 8:-.
172. Recoil reactions in neutron-activation analysis. By D. Brune. 1965. 24 p. Sw. cr. 8:-.
173. A parametric study of a constant-Mach-number MHD generator with nuclear ionization. By J. Braun. 1965. 23 p. Sw. cr. 8:-.
174. Improvements in applied gamma-ray spectrometry with germanium semiconductor detector. By D. Brune, J. Dubois and S. Hellström. 1965. 17 p. Sw. cr. 8:-.
175. Analysis of linear MHD power generators. By E. A. Witalis. 1965. 37 p. Sw. cr. 8:-.
176. Effect of buoyancy on forced convection heat transfer in vertical channels - a literature survey. By A. Bhattacharyya. 1965. 27 p. Sw. cr. 8:-.
177. Burnout data for flow of boiling water in vertical round ducts, annuli and rod clusters. By K. M. Becker, G. Hernborg, M. Bode and O. Erikson. 1965. 109 p. Sw. cr. 8:-.
178. An analytical and experimental study of burnout conditions in vertical round ducts. By K. M. Becker. 1965. 161 p. Sw. cr. 8:-.
179. Hindered EI transitions in Eu^{155} and Tb^{161} . By S. G. Malmkog. 1965. 19 p. Sw. cr. 8:-.
180. Photomultiplier tubes for low level Cerenkov detectors. By O. Strindehag. 1965. 25 p. Sw. cr. 8:-.
181. Studies of the fission integrals of U^{235} and Pu^{239} with cadmium and boron filters. By E. Hellstrand. 1965. 32 p. Sw. cr. 8:-.
182. The handling of liquid waste at the research station of Studsvik, Sweden. By S. Lindhe and P. Linder. 1965. 18 p. Sw. cr. 8:-.
183. Mechanical and instrumental experiences from the erection, commissioning and operation of a small pilot plant for development work on aqueous reprocessing of nuclear fuels. By K. Jönsson. 1965. 21 p. Sw. cr. 8:-.
184. Energy dependent removal cross-sections in fast neutron shielding theory. By H. Grönroos. 1965. 75 p. Sw. cr. 8:-.
185. A new method for predicting the penetration and slowing-down of neutrons in reactor shields. By L. Hjärne and M. Leimdörfer. 1965. 21 p. Sw. cr. 8:-.
186. An electron microscope study of the thermal neutron induced loss in high temperature tensile ductility of Nb stabilized austenitic steels. By R. B. Roy. 1965. 15 p. Sw. cr. 8:-.
187. The non-destructive determination of burn-up means of the Pr-144 2.18 MeV gamma activity. By R. S. Forsyth and W. H. Blackadder. 1965. 22 p. Sw. cr. 8:-.
188. Trace elements in human myocardial infarction determined by neutron activation analysis. By P. O. Wester. 1965. 34 p. Sw. cr. 8:-.
189. An electromagnet for precession of the polarization of fast-neutrons. By O. Aspelund, J. Björkman and G. Trumpy. 1965. 28 p. Sw. cr. 8:-.
190. On the use of importance sampling in particle transport problems. By B. Eriksson. 1965. 27 p. Sw. cr. 8:-.
191. Trace elements in the conductive tissue of beef heart determined by neutron activation analysis. By P. O. Wester. 1965. 19 p. Sw. cr. 8:-.
192. Radiolysis of aqueous benzene solutions in the presence of inorganic oxides. By H. Christensen. 12 p. 1965. Sw. cr. 8:-.
193. Radiolysis of aqueous benzene solutions at higher temperatures. By H. Christensen. 1965. 14 p. Sw. cr. 8:-.
194. Theoretical work for the fast zero-power reactor FR-0. By H. Häggblom. 1965. 46 p. Sw. cr. 8:-.
195. Experimental studies on assemblies 1 and 2 of the fast reactor FR0. Part 1. By T. L. Andersson, E. Hellstrand, S-O. Londen and L. I. Tirén. 1965. 45 p. Sw. cr. 8:-.
196. Measured and predicted variations in fast neutron spectrum when penetrating laminated Fe-D₂O. By E. Aalto, R. Sandlin and R. Fräki. 1965. 20 p. Sw. cr. 8:-.
197. Measured and predicted variations in fast neutron spectrum in massive shields of water and concrete. By E. Aalto, R. Fräki and R. Sandlin. 1965. 27 p. Sw. cr. 8:-.
198. Measured and predicted neutron fluxes in, and leakage through, a configuration of perforated Fe plates in D₂O. By E. Aalto. 1965. 23 p. Sw. cr. 8:-.
199. Mixed convection heat transfer on the outside of a vertical cylinder. By A. Bhattacharyya. 1965. 42 p. Sw. cr. 8:-.
200. An experimental study of natural circulation in a loop with parallel flow test sections. By R. P. Mathisen and O. Eklind. 1965. 47 p. Sw. cr. 8:-.
201. Heat transfer analogies. By A. Bhattacharyya. 1965. 55 p. Sw. cr. 8:-.
202. A study of the "384" KeV complex gamma emission from plutonium-239. By R. S. Forsyth and N. Ronqvist. 1965. 14 p. Sw. cr. 8:-.
203. A scintillometer assembly for geological survey. By E. Dissing and O. Landström. 1965. 16 p. Sw. cr. 8:-.
204. Neutron-activation analysis of natural water applied to hydrogeology. By O. Landström and C. G. Wenner. 1965. 28 p. Sw. cr. 8:-.
205. Systematics of absolute gamma ray transition probabilities in deformed odd-A nuclei. By S. G. Malmkog. 1965. 60 p. Sw. cr. 8:-.
206. Radiation induced removal of stacking faults in quenched aluminium. By U. Bergenlid. 1965. 11 p. Sw. cr. 8:-.
207. Experimental studies on assemblies 1 and 2 of the fast reactor FR0. Part 2. By E. Hellstrand, T. Andersson, B. Brunfelter, J. Kockum, S-O. Londen and L. I. Tirén. 1965. 50 p. Sw. cr. 8:-.
208. Measurement of the neutron slowing-down time distribution at 1.46 eV and its space dependence in water. By E. Möller. 1965. 29 p. Sw. cr. 8:-.
209. Incompressible steady flow with tensor conductivity leaving a transverse magnetic field. By E. A. Witalis. 1965. 17 p. Sw. cr. 8:-.
210. Methods for the determination of currents and fields in steady two-dimensional MHD flow with tensor conductivity. By E. A. Witalis. 1965. 13 p. Sw. cr. 8:-.
211. Report on the personnel dosimetry at AB Atomenergi during 1964. By K. A. Edvardsson. 1966. 15 p. Sw. cr. 8:-.
212. Central reactivity measurements on assemblies 1 and 3 of the fast reactor FR0. By S-O. Londen. 1966. 58 p. Sw. cr. 8:-.
213. Low temperature irradiation applied to neutron activation analysis of mercury in human whole blood. By D. Brune. 1966. 7 p. Sw. cr. 8:-.
214. Characteristics of linear MHD generators with one or a few loads. By E. A. Witalis. 1966. 16 p. Sw. cr. 8:-.
215. An automated anion-exchange method for the selective sorption of five groups of trace elements in neutron-irradiated biological material. By K. Samsahl. 1966. 14 p. Sw. cr. 8:-.
216. Measurement of the time dependence of neutron slowing-down and thermalization in heavy water. By E. Möller. 1966. 34 p. Sw. cr. 8:-.
217. Electrodeposition of actinide and lanthanide elements. By N-E. Barring. 1966. 21 p. Sw. cr. 8:-.
218. Measurement of the electrical conductivity of He³ plasma induced by neutron irradiation. By J. Braun and K. Nygaard. 1966. 37 p. Sw. cr. 8:-.
219. Phytoplankton from Lake Magelungen, Central Sweden 1960-1963. By T. Willén. 1966. 44 p. Sw. cr. 8:-.
220. Measured and predicted neutron flux distributions in a material surrounding a cylindrical duct. By J. Nilsson and R. Sandlin. 1966. 37 p. Sw. cr. 8:-.
221. Swedish work on brittle-fracture problems in nuclear reactor pressure vessels. By M. Grounes. 1966. 34 p. Sw. cr. 8:-.
222. Total cross-sections of U, UO₂ and ThO₂ for thermal and subthermal neutrons. By S. F. Beshai. 1966. 14 p. Sw. cr. 8:-.
223. Neutron scattering in hydrogenous moderators, studied by the time dependent reaction rate method. By L. G. Larsson, E. Möller and S. N. Purohit. 1966. 26 p. Sw. cr. 8:-.
224. Calcium and strontium in Swedish waters and fish, and accumulation of strontium-90. By P-O. Agnedal. 1966. 34 p. Sw. cr. 8:-.
225. The radioactive waste management at Studsvik. By R. Hedlund and A. Lindskog. 1966. 14 p. Sw. cr. 8:-.
226. Theoretical time dependent thermal neutron spectra and reaction rates in H₂O and D₂O. S. N. Purohit. 1966. 62 p. Sw. cr. 8:-.
227. Integral transport theory in one-dimensional geometries. By I. Carlvik. 1966. 65 p. Sw. cr. 8:-.
228. Integral parameters of the generalized frequency spectra of moderators. By S. N. Purohit. 1966. 27 p. Sw. cr. 8:-.
229. Reaction rate distributions and ratios in FR0 assemblies 1, 2 and 3. By T. L. Andersson. 1966. 50 p. Sw. cr. 8:-.
230. Different activation techniques for the study of epithermal spectra, applied to heavy water lattices of varying fuel-to-moderator ratio. By E. K. Sokolowski. 1966. 34 p. Sw. cr. 8:-.
231. Calibration of the failed-fuel-element detection systems in the Ågesta reactor. By O. Strindehag. 1966. 52 p. Sw. cr. 8:-.
232. Progress report 1965. Nuclear chemistry. Ed. by G. Carleson. 1966. 26 p. Sw. cr. 8:-.
233. A Summary Report on Assembly 3 of FR0. By T. L. Andersson, B. Brunfelter, P. F. Cecchi, E. Hellstrand, J. Kockum, S-O. Londen and L. I. Tirén. 1966. 34 p. Sw. cr. 8:-.
234. Recipient capacity of Tvären, a Baltic Bay. By P-O. Agnedal and S. O. W. Bergström. 21 p. Sw. cr. 8:-.
235. Optimal linear filters for pulse height measurements in the presence of noise. By K. Nygaard. 16 p. Sw. cr. 8:-.
236. DETEC, a subprogram for simulation of the fast-neutron detection process in a hydro-carbonous plastic scintillator. By B. Gustafsson and O. Aspelund. 1966. 26 p. Sw. cr. 8:-.
237. Microanalysis of fluorine contamination and its depth distribution in zircaloy by the use of a charged particle nuclear reaction. By E. Möller and N. Starfelt. 1966. 15 p. Sw. cr. 8:-.
238. Void measurements in the regions of sub-cooled and low-quality boiling. P. 1. By S. Z. Rouhani. 1966. 47 p. Sw. cr. 8:-.
239. Void measurements in the regions of sub-cooled and low-quality boiling. P. 2. By S. Z. Rouhani. 1966. 60 p. Sw. cr. 8:-.
240. Possible odd parity in ¹³⁵Xe. By L. Broman and S. G. Malmkog. 1966. 10 p. Sw. cr. 8:-.
241. Burn-up determination by high resolution gamma spectrometry: spectra from slightly-irradiated uranium and plutonium between 400-830 keV. By R. S. Forsyth and N. Ronqvist. 1966. 22 p. Sw. cr. 8:-.
242. Half life measurements in ¹⁵²Gd. By S. G. Malmkog. 1966. 10 p. Sw. cr. 8:-.
243. On shear stress distributions for flow in smooth or partially rough annuli. By B. Kjellström and S. Hedberg. 1966. 66 p. Sw. cr. 8:-.

Förteckning över publicerade AES-rapporter

- Analys medelst gamma-spektrometri. Av D. Brune. 1961. 10 s. Kr 6:-.
 - Bestrålningförändringar och neutronatmosfär i reaktortrycktankar - några synpunkter. Av M. Grounes. 1962. 33 s. Kr 6:-.
 - Studium av sträckgränsen i mjukt stål. Av G. Östberg och R. Attermo. 1963. 17 s. Kr 6:-.
 - Teknisk upphandling inom reaktorområdet. Av Erik Jonson. 1963. 64 s. Kr 8:-.
 - Ågesta Kraftvärmeverk. Sammanställning av tekniska data, beskrivningar m. m. för reaktor delen. Av B. Lilliehöök. 1964. 336 s. Kr 15:-.
 - Atomdagen 1965. Sammanställning av föredrag och diskussioner. Av S. Sandström. 1966. 321 s. Kr 15:-.
- Additional copies available at the library of AB Atomenergi, Studsvik, Nyköping, Sweden. Micronegatives of the reports are obtainable through the International Documentation Center, Tumba, Sweden.